Fusion Journal of Engineering and Sciences

Technical Article.

Vibration Control through Multiple Tuned Mass Dampers

Aaqib Najeeb [1, *], Taimoor Shehzad [1], MD Nowsad Islam [2] and Hassan Ayaz [3]

[1] Department of Structural Engineering, College of Civil Engineering, Tongji University, Shanghai,200092, China; aaqib_najeeb@tongji.edu; taimoor@tongji.edu.cn.
[2] Department of Bridge Engineering, College of Civil Engineering, Tongji University, Shanghai,200092, China; nowsad@tongji.edu.cn.
[3] Department of Geotechnical Engineering, Tongji University, Shanghai 200092, China; 2393163@tongji.edu.cn
* Correspondence: aaqib_najeeb@tongji.edu; Tel.: (+86-18921901659)

Abstract

Structural responses under dynamic loading contain multiple frequency components, which can excite several vibration modes simultaneously. Among passive dynamic vibration absorbers (DVAs), tuned mass dampers (TMDs) are the most widely used. In practice, a single TMD (STMD) is typically installed at the roof to target the fundamental mode, leaving higher modes insufficiently controlled and limiting overall effectiveness. This study investigates multi-TMD (MTMD) configurations to enhance multimodal vibration mitigation. Three layouts are examined: (i) distributed MTMDs (d-MTMDs), placed according to mode shapes; (ii) arbitrary MTMDs (a-MTMDs), positioned without placement rules; and (iii) roof-clustered MTMDs (MTMDs@top), all devices located at the top. The STMD is tested on a 20-degree-of-freedom (DOF) shear-building model, while all MTMD configurations are applied to an 80-DOF benchmark structure. Governing equations of motion are derived analytically and solved numerically using the Newmark-β linear acceleration method. The 20-DOF system is subjected to recorded earthquake excitations, and the 80-DOF to wind histories. Performance is evaluated using square-root-sum-of-squares (SRSS) and root-mean-square (RMS) metrics. Results show that d-MTMDs achieve the most effective multimodal control, whereas a-MTMDs provide comparable global reductions to MTMDs@top but less consistent mitigation in upper stories.

Keywords: Single TMD; Multiple TMDs; Shear-building model; Newmark-β integration method; Multimodal vibration control; earthquake excitations; wind histories.

1. Introduction

The trend toward constructing taller structures has increased rapidly over the past decade. Tall buildings can accommodate a significantly larger population compared to low-rise structures occupying the same land area. Consequently, they are considered more suitable from the perspectives of sustainability, land-use efficiency, and economic viability, and they offer a practical solution to the growing demand for urban accommodation driven by rapid population growth. However, tall structures are generally characterized by high flexibility and low natural frequencies, which result in low inherent damping and long vibration durations during dynamic excitations. These characteristics make them highly susceptible to excessive vibrations induced by wind and seismic loads, thereby increasing the risk of structural damage, occupant discomfort, and failure of sensitive nonstructural components. Therefore, vibration control becomes a critical requirement for ensuring both structural safety and serviceability.

In general, two main categories of measures are adopted to control excessive structural oscillations under wind, earthquake, or other dynamic loadings. The first category consists of local measures, which involve improving specific structural components by modifying material properties or sectional geometry of individual members. Although such enhancements can improve local performance, their influence on the overall global dynamic response of the structure remains limited. Some localized vibration control devices can also be employed to reduce the response of individual structural elements; however, their effect on the global behavior of the entire structural system is relatively small. Hence, global vibration control measures are required to achieve effective overall mitigation.

At the global level, vibration control strategies are generally classified into three main types: active, passive, and hybrid control systems. Active systems require continuous external energy input for their operation, whereas passive systems function without any external power source. Hybrid systems combine the characteristics of both active and passive control. Among these, passive control systems are the most widely adopted in engineering practice due to their simplicity, reliability, cost-effectiveness, and low maintenance requirements. Most passive control devices exhibit linear behavior and are typically tuned to a specific structural frequency to achieve optimal vibration suppression.

However, wind and seismic excitations are stochastic in nature, with frequency contents that are random and distributed over a wide spectrum. Consequently, these excitations can simultaneously activate multiple vibration modes of a structure. This behavior is particularly pronounced in tall and slender buildings, where higher-mode contributions become significant compared to low-rise structures.

2. Background

The problem of structural vibration has long been recognized as a critical issue in engineering practice. It has been widely observed in earlier generations of structures subjected to dynamic excitations such as wind, waves, rotating machinery, and seismic ground motion. The phenomenon of vibration is not confined to structural engineering alone; it also represents a fundamental concern in other disciplines such as mechanical, aerospace, and marine engineering. Consequently, extensive theoretical and experimental investigations have been conducted over the past century to develop effective strategies for vibration suppression and motion control of dynamically sensitive systems.

A TMD is a classical passive vibration control device comprising a secondary mass, an elastic element that provides stiffness, and a viscous damping component, all connected to the primary structure. Its working principle is based on generating an out-of-phase inertial force that counteracts the motion of the main structure, thereby reducing its dynamic response. Because of its simple configuration, robustness, and cost-effectiveness, the TMD has become one of the most widely adopted passive control devices in modern structural design. It enhances damping capacity, ensures stable performance under varying environmental conditions, and improves both structural serviceability and occupant comfort.

The earliest recorded application of a TMD was by Frahm (1909), who employed a STMD to control ship rolling and minimize oscillations at a target frequency [1]. The device, consisting of a small auxiliary mass connected to the main structure by a linear spring, was effective only within a narrow frequency band. Later, Ormondroyd and Den Hartog (1928) refined the concept by incorporating damping into the device, thereby broadening its operational bandwidth and introducing the concept of invariant points for optimal tuning of absorber and structural responses. Den Hartog (1956) subsequently formalized the theoretical foundation of the STMD for undamped primary systems in his

seminal work [2]. However, under broadband excitations such as earthquake loading, the performance of an STMD deteriorates significantly and may even amplify the response due to dynamic coupling between the primary and secondary systems [3]. Although the Tuned Mass Damper Inerter (TMDI) offers a wider operational bandwidth than a conventional TMD, it remains sensitive to detuning effects similar to those of traditional systems [4].

Another well-established passive vibration control device is the Tuned Liquid Damper (TLD), which consists of a partially filled tank whose first sloshing mode is tuned to the fundamental frequency of the structure. As the structure moves, the liquid sloshes and generates out-of-phase inertial forces that dissipate energy, thereby reducing vibrations. Designing TLDs, however, is challenging because the liquid-sloshing behavior is inherently nonlinear. A state-of-the-art approach, Real-Time Hybrid Testing (RTHT) [5], has emerged as a feasible solution for evaluating TLD performance, though it is not universally applicable to all structures requiring vibration control. Furthermore, TLDs suffer from the same detuning problem as TMDs, since they must be tuned to a particular single mode. Practical testing is also preferred over numerical or finite-element analyses for accuracy, but such testing is not always feasible [6]. A recent study employed machine learning techniques to predict the dynamic response of liquid tanks; however, the liquid mass was modeled as an equivalent single-degree-of-freedom (SDOF) system, which could not fully capture higher-order sloshing modes and nonlinear fluid–structure interactions [7].

In addition to TMDs and TLDs, other passive control devices such as; base isolators, viscous and particle dampers, pendulum absorbers, shock absorbers, and rocking-mass absorbers have also been widely used. In all these devices, the tuning process involves matching the natural frequency of the absorber with that of the target structural mode. When the tuning is accurate, the absorber effectively draws energy from the structure and suppresses vibration. However, detuning remains a significant drawback. If the excitation frequency changes or if the input contains multiple strong frequency components (as in broadband excitation), the effectiveness of the device diminishes sharply.

To overcome these limitations, the concept of MTMDs was introduced. Initially used in mechanical systems during the late 1970s, MTMDs consist of several smaller TMD units, each tuned to slightly different frequencies. This distributed tuning broadens the effective frequency bandwidth and reduces sensitivity to mistuning, enhancing robustness under multi-mode and non-stationary excitations. Ayorinde and Warburton (1980) were among the first to extend the application of MTMDs from mechanical to civil structures [8]. Their analytical and experimental results showed that two or more dampers can achieve superior vibration suppression compared with a single absorber [9]. Kareem and Kline (1995) further studied MTMDs under random or uncertain loading and demonstrated that multiple smaller dampers, collectively equivalent in total mass to a single large one, offer improved control performance and easier handling and installation, making them suitable for retrofitting applications [10].

Subsequent research significantly advanced MTMD design. Ram and Elhay (1996) distributed the natural frequencies of individual dampers around the fundamental mode of the main structure, thereby minimizing detuning effects [11]. Joshi and Jangid (1997) optimized MTMD parameters and found that, for an equal total mass ratio, an MTMD system outperforms an STMD [12]. Jangid (1995, 1999) further investigated optimal parameters for undamped primary structures [13,14]. Blondel and Tsitsiklis (2000) emphasized the complexity of MTMD optimization due to the large number of interdependent variables [15]. Later studies by Li (2000, 2002, 2003) confirmed that optimally designed MTMDs offer enhanced robustness and efficiency over STMDs [16–18]. Park and Reed (2001) analyzed uniformly and linearly distributed MTMDs under harmonic excitation, accounting for redundancy effects, while Li and Liu (2002–2004) compared various

MTMD configurations under constraints on mass, stiffness, and damping. Wen and Zou (2003) developed a frequency-domain framework for analyzing multi-storey structures equipped with MTMDs, providing deeper insight into their dynamic performance [19].

Building on these foundations, Li and Zhang (2005) [20], Li and Li (2005) [21], Han and Li (2006) [22], and Li (2006) [23] proposed MTMDs with distributed natural frequencies for enhanced control efficiency. Li and Zhu (2006) showed that Double Tuned Mass Dampers (DTMDs) can outperform conventional MTMDs [24], while Li and Ni (2007) demonstrated that optimized, non-uniformly distributed d-MTMDs are more effective than uniformly distributed systems [25]. Han and Li (2006, 2008) concluded that MTMDs with identical stiffness and damping but unequal masses and uniformly spaced natural frequencies achieve superior control [26,27]. Ok, Song, and Park (2009) proposed design formulas for bi-tuned mass dampers that ensure both nominal and robust performance under seismic loading [28]. A comprehensive review by Parulekar and Reddy (2009) summarized the evolution of passive control systems for seismic response reduction [29]. Zuo (2009) analytically confirmed the superior effectiveness of MTMDs over single-unit TMDs with the same total mass ratio [30]. Experimental validation by Lin et al. (2010) further demonstrated that optimally designed MTMDs significantly reduce structural vibrations and control damper stroke length [31]. Yang, Munoa, and Altintas (2010) extended MTMD optimization techniques to mechanical systems such as tool clamping assemblies [32], while Jokic, Stegic, and Butkovic (2011) introduced an optimization method based on dissipativity inequalities for tuning MTMDs [33].

Although MTMDs share similar configurations, their spatial placement within the structure critically affects vibration control performance. Researchers have consistently found that increasing the total mass ratio improves damping efficiency under wind and seismic loads. However, concentrating large masses at a single location is often impractical. As a result, spatially distributed configurations have been explored. Bergman et al. (1989) [34] demonstrated the benefit of vertically distributed MTMDs using cantilever beam models, while Feng and Mita (1995) introduced the mega-sub TMD system concept for tall buildings [35]. Sadek et al. (1997) established optimal TMD parameters for seismic loading and showed that equal damping ratios in the first two modes yield improved results for highly damped structures [36]. Chen and Wu (2001) [37] and Wu and Chen (2000) [38] analyzed the influence of TMD placement based on structural acceleration, concluding that MTMDs are particularly effective at reducing acceleration responses in lower stories. Petit, Loccufier, and Aeyels (2009) highlighted the importance of placement optimization by maximizing frequency shifts away from resonance [39].

Further advancements were made by Ali and Moon (2007), who examined vortex-shedding-induced lock-in phenomena in tall buildings [40]. Moon (2010) found that vertically distributing MTMDs according to mode shapes minimizes performance loss [41]. Fu and Johnson (2009, 2011) investigated externally mounted shading-fin TMDs and confirmed that distributed MTMDs outperform conventional systems under historical earthquake records [42,43]. Xiang and Nishitani (2014) demonstrated that MTMDs are effective for multi-mode control in low-rise structures with closely spaced frequencies [44]. Elias and Matsagar (2014a, 2014b) confirmed the superior performance of distributed MTMDs for across-wind vibration control in high-rise benchmark buildings [45,46].

Moon (2015) introduced the TMD/Double-Skin Façade Damping (DSFD) interaction system, addressing space constraints at the roof level and the need for additional mass [47]. This configuration achieved comparable damping ratios with significantly smaller mass requirements. Elias, Matsagar, and Datta (2016, 2017a) further demonstrated that TMDs designed to target multiple modes outperform single-mode designs in chimneys and high-rise buildings under seismic excitation [48,49]. Recent optimization-based studies comparing advanced configurations such as a-MTMDs and d-MTMDs have concluded

that the distributed d-MTMD arrangement provides the most robust performance among all conventional variants [50].

Due to these extensive advancements, TMDs and their derivatives have attracted substantial research and practical interest. They have been successfully implemented in numerous full-scale engineering projects [51], including landmark skyscrapers such as the Taipei 101 Tower and the Shanghai Tower, establishing TMDs and MTMDs as indispensable components of modern structural vibration control systems.

Although extensive research has been carried out on TMD and MTMD systems, several important aspects remain insufficiently explored. Most previous studies have focused on optimizing a single type of MTMD configuration rather than systematically comparing the multimodal vibration control performance of different configurations and also the STMD under identical conditions. The influence of damper placement within the structure has also received limited attention. However, not only the location and the mode to which it is tunned but also the mass ratio of the TMD play a critical role in determining control efficiency. Furthermore, the performance of these devices under sequential wind and earthquake excitations across different structural types has not been comprehensively investigated. Another significant limitation in existing literature is the lack of analysis linking control performance to specific floor levels. Previous studies rarely quantified how much vibration reduction can be achieved at different stories or which damper configuration is most effective for controlling particular floors. In addition, few studies have evaluated global response measures such as overall vibration mitigation (SRSS-based) and peak response reduction, both of which are essential indicators of real structural control efficiency.

To address these gaps, the present study proposes the implementation of a MTMD system for achieving effective multimodal vibration control. The system involves distributing several smaller dampers at strategically selected locations within the structure, each tuned to an appropriate modal frequency and mass ratio to optimize control performance across multiple modes. Various MTMD configuration schemes are examined and compared through a detailed case study to assess both global and story-wise vibration response control. In this study, two structural models are considered to comprehensively evaluate the proposed control strategy. The first is a 20-story building subjected to earthquake excitations and controlled using STMD. The second is an 80-story high-rise structure exposed to wind-induced dynamic loads and equipped with either STMD and MTMDs configurations. The comparative performance of these systems is analyzed in terms of peak and RMS response reductions, as well as overall vibration mitigation efficiency. The outcomes of this investigation are expected to demonstrate the superior robustness and reliability of the MTMD system for mitigating multimodal vibrations under diverse dynamic loading conditions.

3. Methodology

The methodology adopted in this study is structured into three major phases: Modelling Phase (Part #1), Optimization Phase (Part #2), and Selection Phase (Part #3). Each phase is composed of a sequence of analytical, numerical, and decision-making steps, collectively designed to determine the optimal vibration-control configuration for multi-degree-of-freedom (MDOF) structures under dynamic excitation. The overall framework integrates structural dynamics, TMD theory, and dynamics analysis within a systematic workflow, as illustrated in Figure 1.

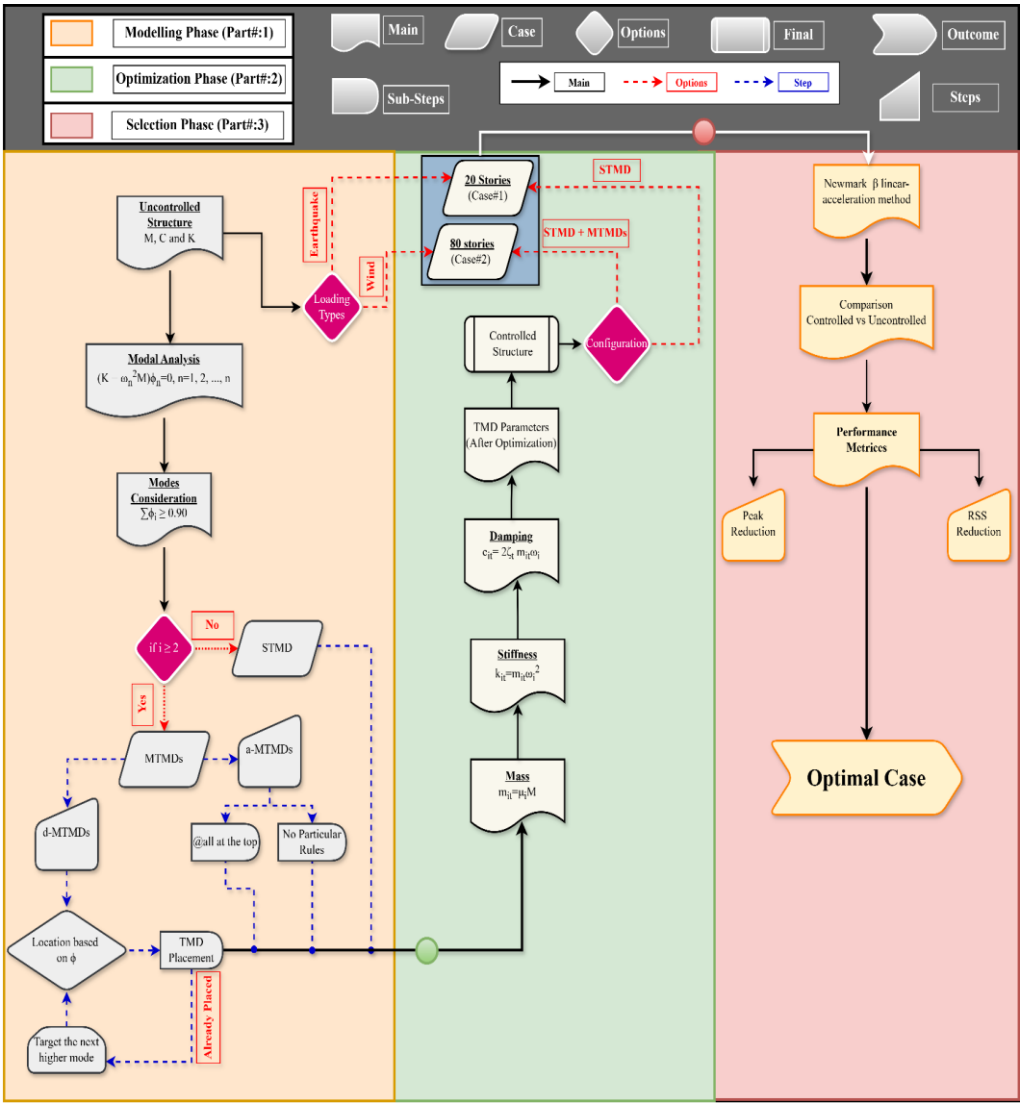

Figure 1. Methodological flowchart of the study.

1.1 *Modelling Phase*

The modelling phase establishes the foundation of the study by developing the structural model and determining its modal characteristics before the introduction of any control mechanism. The objective of this stage is to define the dynamic properties of the uncontrolled structure, which serve as the reference baseline for subsequent comparisons with the controlled cases.

In this phase, the structure was idealized as a shear-type MDOF system represented by three fundamental matrices: the global mass matrix (M), the damping matrix (C), and the stiffness matrix (K). These matrices are formulated based on realistic physical parameters, including story masses, inter-story stiffnesses, and damping ratios that correspond to practical building systems. Two structural models are considered in this study. The first is a twenty-story frame representing a medium-rise building (Case #1), and the second is an eighty-story frame representing a high-rise building (Case #2). This dual-case modelling approach allows a comparative investigation of TMD performance across different height categories and loading types namely earthquake and wind histories.

Once the structural model is defined, modal analysis is performed to obtain the natural frequencies and corresponding mode shapes of the structure. The vibration

characteristics are determined by solving the classical eigenvalue problem as shown in the equation 1:

$$(K - \omega_n^2 M)\,\phi_n = 0, \quad n = 1,2,\dots,N \tag{1}$$

Where ω_n is the natural circular frequency of the nth mode and ϕ_n is its corresponding mode shape vector. The resulting modal parameters are then used to compute the modal mass participation ratios, which quantify the contribution of each mode to the total dynamic response of the structure. Only those modes that collectively contribute more than ninety percent of the total effective mass should be retained for further analysis, ensuring computational efficiency while preserving accuracy. This requirement can be expressed mathematically as show in the equation 2:

$$\sum_{n=1}^{i} \beta_n^2 \geq 0.90 \tag{2}$$

where β_n denotes the modal participation factor of the nth mode. After identifying the dominant modes, a mode-based decision criterion is applied to determine the appropriate control strategy. If the structure is mainly controlled by one or two dominant modes ($i \leq 2$), a STMD configuration is selected to target the most critical mode(s). However, if more than two modes are dynamically significant ($i > 2$), a MTMD configuration is adopted, as it can simultaneously address several closely spaced modes and provide broader vibration suppression capability.

When the MTMD approach is required, three distinct configurations are investigated. The first configuration, termed a-MTMDs, distributes the natural frequencies of the dampers without any fixed spatial or frequency rule, offering flexibility but introducing some uncertainty in performance. The second configuration, known as d-MTMDs, arranges the dampers according to the amplitude of the structural mode shapes, thereby enhancing energy dissipation across different modes. In case damper is already present in the selected location of a mode then the damper is specifically tuned to target the next higher mode for more effective control of multi-modal vibrations.

The placement of dampers is another crucial step within the modelling phase. For the distributed MTMD configuration, the dampers are located at positions corresponding to the maximum amplitude of the selected mode shapes, ensuring that they act most effectively at points of peak modal displacement. In configurations where dampers are installed only at the roof level, such as in the STMD and MTMD@roof cases, placement is kept uniform to enable a consistent basis for comparison among configurations. Figure 2 illustrates the typical configuration of both the uncontrolled (Figure 2a) and controlled structures (Figure 2b). While the figure shows the STMD and a single MTMD placement, in this study, the MTMDs are arranged in multiple configurations

1.2 Optimization Phase

The optimization phase focuses on determining the optimal mechanical properties of the TMD systems for maximum vibration reduction efficiency. This phase begins with the assembly of the controlled structural system, where the selected TMD configuration either STMD or one of the MTMD variants is coupled to the primary structure. The coupled equations of motion of the coupled system are formulated to include both structural and absorber degrees of freedom, ensuring that their dynamic interactions are fully captured.

The optimization process then proceeds to the determination of TMD parameters, namely mass (m_t), stiffness (k_t), and damping (c_t). These parameters are defined by analytical relations and refined through numerical optimization. The mass of the tuned

damper is expressed as equation 3 where μ denotes the mass ratio representing the proportion of the auxiliary damper mass relative to the total mass of the structure. The stiffness of the TMD is calculated using equation 4 where ω_t is the tuning frequency of the damper, typically selected to coincide with or near the dominant frequency of the controlled mode. The damping coefficient of the damper is determined as equation 5 where ζ_t is the damping ratio of the TMD, optimized either through closed-form expressions (such as those based on Den Hartog tuning) or through iterative numerical procedures aimed at minimizing the overall response:

$$m_t = \mu M; \tag{3}$$

$$k_t = m_t \omega_t^2 \tag{4}$$

$$c_t = 2\zeta_t \sqrt{k_t m_t} \tag{5}$$

To evaluate the time-domain response of the controlled system, the coupled equations of motion (equation 6) are solved using the Newmark-β linear acceleration method. This integration scheme allows step-by-step computation of displacements, velocities, and accelerations under arbitrary time-dependent external loading, making it particularly suitable for both seismic and wind excitations. Here the $x, \dot{x}$ *and* $\ddot{x}$ show the displacement, velocity and acceleration of the system. $\ddot{x_g}$ is ground acceleration and r is the effective seismic force distribution vector.

$$M\,\ddot{x}(t) + C\,\dot{x}(t) + K\,x(t) = -M\,r\,\ddot{x_g}(t)$$

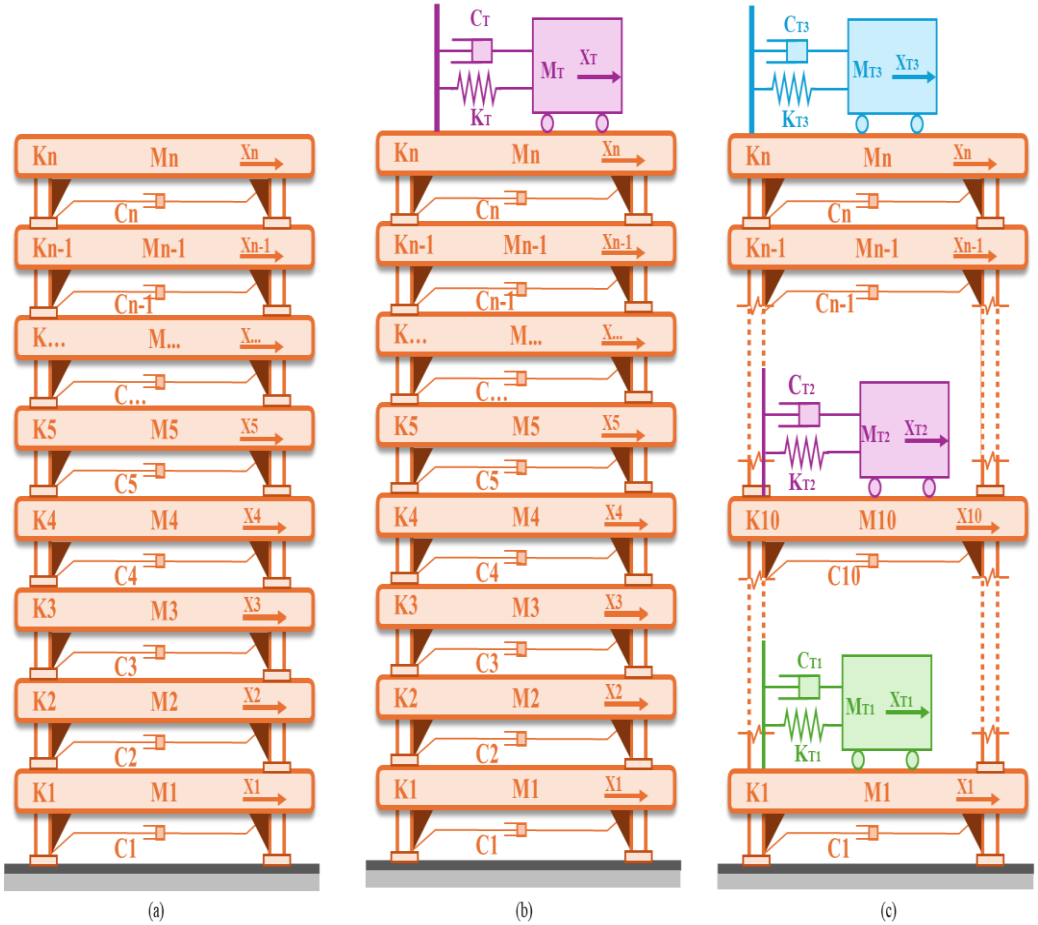

Figure 2. (a) Uncontrolled structured and structure controlled with: **(b)** STMD and **(c)** MTMDs.

The equation 7 presents the parameters of the uncontrolled primary structure. equation 8 presents the parameters corresponding exclusively to the TMD. In addition, equation 9 provides the attachment matrix associated with the TMD. equations 10, 11, and 12 represent the full mass, damping, and stiffness matrices, respectively.

Let the structural system (without TMDs) have the following matrices:

$$M_s,\ C_s, K_s \in \mathbb{R}^{(n\times n)} \tag{7}$$

The diagonal matrices of the TMD parameters are defined as:

$$M_{T=}\, diag\left(m_{T1,\ \ldots\ldots}, m_{Tp}\right), C_{T=}\, diag\left(c_{T1,\ \ldots\ldots}, c_{Tp}\right), K_{T=}\, diag\left(k_{T1,\ \ldots\ldots}, k_{Tp}\right) \tag{8}$$

The attachment selection matrix $B \in \mathbb{R}^{(n\times p)}$ is defined as:

$$B_{ij} = \begin{cases} 1, & if\ the\ j^{th}\ TMD\ is\ attached\ to\ i^{th} structural\ DOF, \\ 0, & otherwise \end{cases} \tag{9}$$

The global mass, damping, and stiffness matrices of the coupled structure–TMD system can then be written as:

$$\mathbf{M} = \begin{bmatrix} M_s & \\ & M_T \end{bmatrix} \tag{10}$$

$$\mathbf{C} = \begin{bmatrix} C_s + B\ C_T B^T & -B\ C_T \\ -\ C_T B^T & C_T \end{bmatrix} \tag{11}$$

$$\mathbf{K} = \begin{bmatrix} K_s + B\ K_T K^T & -B\ K_T \\ -\ K_T B^T & K_T \end{bmatrix} \tag{12}$$

An iterative optimization loop is then established to refine the TMD parameters. Within this loop, the structural response is calculated for each set of candidate parameters, and performance metrics such as displacement, acceleration, and inter-story drift are extracted. The process continues until convergence is achieved toward an optimal combination of damper mass, stiffness, and damping that minimizes the global vibration response while maintaining structural feasibility. The equation 13 represents the Newmark-beta formula used to compute the structural displacement at the next time step in dynamic analysis. Here the Δt is the time step while β is the Newmark parameter that controls numerical stability and accuracy (β = 0.1667 for linear while 0.25 for average acceleration method).

$$x_{t+\Delta t} = x_t + \Delta t\, \dot{x}_t + \frac{\Delta t^2}{2}[(1-2\beta)\, \ddot{x}_t + 2\beta\, \ddot{x}_{t+\Delta t}] \tag{13}$$

The Figure 3 illustrates nonzero entry patterns after coupling MTMDs with the main structural matrices. Subfigures (a) and (b) illustrate the distribution of nonzero elements in C and K of the structure when MTMDs are placed at the roof level. The patterns confirm

the localized coupling effect, where the interaction is primarily concentrated near the upper degrees of freedom. Subfigures (c) and (d) show the corresponding nonzero patterns for the d-MTMD configuration. In this case, the coupling extends across several degrees of freedom, resulting in a broader spread of nonzero entries in both C and K. This indicates that the d-MTMD arrangement enhances modal participation and energy dissipation throughout the structure rather than being confined to a single level.

In addition, the Figure 4 shows coupling effects on the M, C, and K of the main structure for the MTMD and d-MTMD configurations. Panels (a)–(c) present the M, C, and K matrices of the d-MTMD system. Panels (d)–(f) display the same metrics but for MTMDs@roof. The panels (g)–(i) depict the coupling effects in the M, C and K of the d-MTMD system, while panels (j)–(l) also highlight the coupling effects but in the case of MTMDs@roof. The added mass (ΔM), damping coupling (ΔC), and stiffness coupling (ΔK) components are most pronounced near the upper degrees of freedom, indicating localized influence. Comparatively, the d-MTMD case exhibits a more evenly distributed coupling across the structural height, which enhances modal energy transfer and control performance.

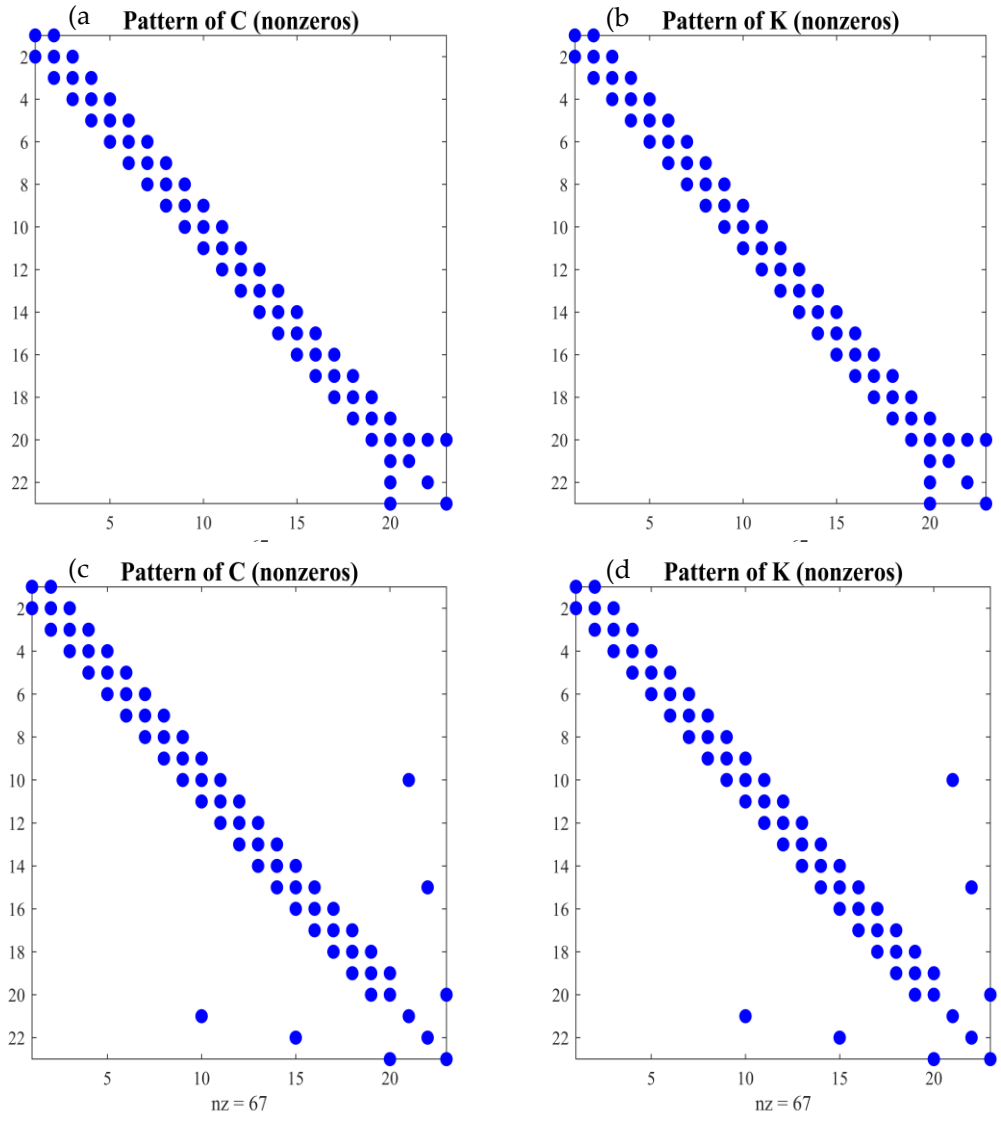

Figure 3. Nonzero entries after coupling MTMDs with the main structure matrices. (a) Stiffness and (b) damping matrices for MTMDs@roof; (c) and (d) show the corresponding results for the d-MTMD.

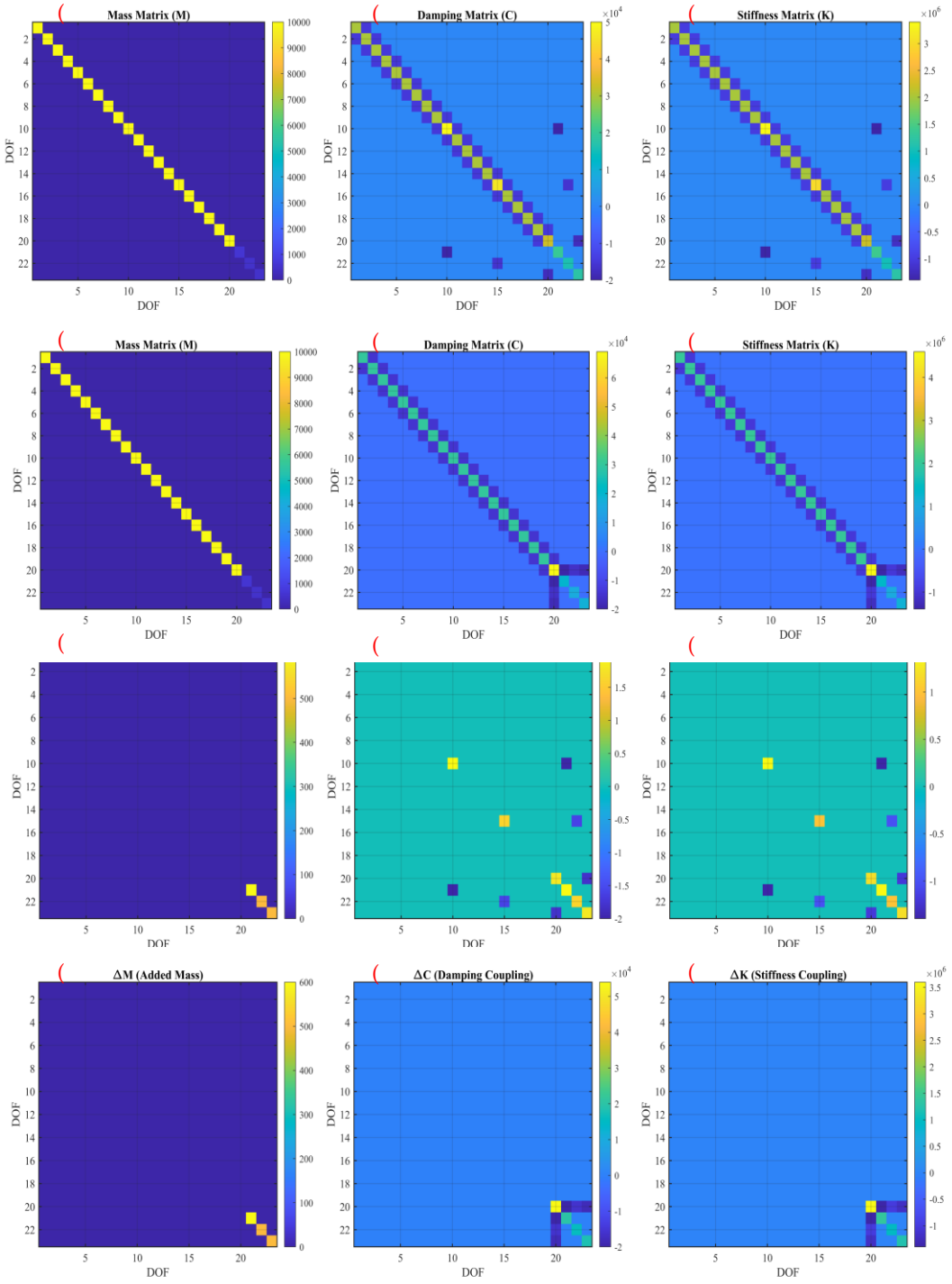

Figure 4. (a)–(c) M, C, and K matrices for the d-MTMDs configuration; (d)–(f) the corresponding matrices for the MTMDs@roof configuration. Likewise, (g)–(i) and (j)–(l) illustrate the coupling-induced modifications in the matrices for the d-MTMDs and MTMDs@roof cases, respectively.

1.3 Selection Phase

The final phase of the methodology involves performance evaluation and optimal configuration selection. In this phase, the dynamic responses of the controlled and uncontrolled structures are compared quantitatively under the same excitation conditions to assess the efficiency of each control configuration.

The comparison focuses on two principal performance metrics. The first metric is Peak Reduction, which measures the ratio of the maximum displacement or acceleration in the controlled system to that in the uncontrolled case. This metric provides a direct indication of the damper's ability to suppress the most critical response amplitude. The second metric is the Root-Sum-Square (RSS) Reduction, which evaluates the overall reduction in the cumulative energy content of the structural response. It is computed as the SRSS responses over the entire time history, thereby representing the integrated vibration energy dissipation achieved by the control system.

Based on these performance indices, all controlled configurations are ranked, and the case exhibiting the greatest improvement in both peak and RSS reductions is designated as the optimal case. This optimal configuration represents the most efficient combination of mass ratio, stiffness, and damping ratio under the given dynamic conditions, achieving the best compromise between performance, stability, and practical feasibility. The equation 14 represent the peak and RSS response ratios of the controlled and uncontrolled structures, and the percentage reduction is calculated as one minus the ratio multiplied by 100.

$$R_{\text{peak}} = \frac{x_{\text{max,controlled}}}{x_{\text{max,uncontrolled}}}$$

$$R_{\text{RSS}} = \frac{\sqrt{\sum_{i=1}^{N} x_{i,\text{controlled}}^2}}{\sqrt{\sum_{i=1}^{N} x_{i,\text{uncontrolled}}^2}} \tag{14}$$

3. Results and Discussion

The results of this study include two structural systems as mentioned earlier. The first is a 20-story building that was subjected to earthquake excitation, and the second is an 80-story high-rise structure that was analyzed under wind loading. It should be noted that the 20-story structure was controlled using a STMD installed at the roof level. In contrast, the 80-story structure showed significant influence of higher modes; therefore, MTMD configurations were considered instead of a single device. The MTMDs were arranged according to three placement strategies. The first was an arbitrary arrangement without a fixed positioning rule. The second was a mode-informed placement where the dampers were installed at the locations corresponding to the maximum modal displacements. The third configuration included several TMDs placed at the roof level. The performance of these MTMD configurations was then compared with each other in terms of vibration reduction and control efficiency when the 80-story structure was subjected to wind-induced excitations.

3.1. Building dynamics and applied loading

Figure 5 (a) illustrates the mode shapes of Case 1, representing a 20-story shear type structure which was subjected to earthquake excitation and controlled by a STMD. The results indicate that the first natural frequency of the system is relatively low, corresponding to the fundamental mode that governs the overall dynamic response due to its high modal participation factor. As the mode number increases, the natural frequencies rise while the participation of each higher mode decreases. Since the fundamental mode dominates the global deformation pattern, particularly in low to mid rise buildings, installing a STMD tuned to this mode is sufficient to achieve effective vibration suppression. In contrast to MTMD systems commonly used in taller or more complex structures, the STMD in this case efficiently mitigates the response concentrated around the first mode resonance. The vertical reference line in the figure represents the nodal axis, and the number

of times each mode shape crosses this line follows the general rule of n minus one crossing, where n denotes the mode number.

Figure 5 (b) shows the mode shapes of Case 2, which represents an 80-story high-rise structure. It is evident that the fundamental time period of this structure is significantly longer than that of the 20-story building in Case 1, as taller structures require more time to complete one vibration cycle due to their increased flexibility. Unlike the previous case, where the first mode dominated the overall response, in this high-rise structure several higher modes also contribute notably to the dynamic behavior. For this reason, MTMDs with different configurations were adopted instead of a STMD to achieve effective vibration control across multiple participating modes. In the figure, the red dots indicate the locations of the installed TMDs corresponding to the distributed d-MTMD arrangement. It is also noted that the fifth mode was excluded from additional control because the maximum response in that mode occurred at a location already equipped with a TMD, and therefore, the design priority was shifted toward suppressing higher modes.

Since the time period of high-rise structures is relatively long, earthquake loading does not usually represent the main challenge for these buildings. Instead, wind loading, which contains lower frequency components that are closer to the natural frequencies of the structure, becomes the dominant factor influencing their dynamic response. Therefore, rather than applying earthquake excitation, which generally involves higher frequency ground motions that are not critical for tall and flexible buildings, the structure in this case was subjected to artificial wind loading, as this represents the primary design concern for high rise structures with respect to serviceability and occupant comfort.

Figure 6 presents the acceleration time histories along with their corresponding Fourier amplitude spectra for the ground motions used in this case study. The blue curves represent how the ground acceleration changes with time, while the red curves display the Fourier amplitudes, highlighting the distribution of energy across different frequencies. For clearer visualization, the Fourier amplitude spectrum of each ground motion is placed directly below its respective time history, making it easier to observe the relationship between the temporal variation and the frequency content of the same record. Together, these plots provide a complete picture of both the time-dependent behavior and the frequency characteristics of the input motions, which are important for understanding how each earthquake excitation may influence the structural response in terms of both overall and peak performance.

The selected earthquake records show distinct characteristics that reflect the diversity of seismic sources and site conditions. Motions such as El Centro (1940, USA), Kobe (1995, Japan), Loma Prieta (1989, USA), and Hollister (1974, USA) are examples of near-fault earthquakes, where strong pulses and abrupt energy releases are typically observed. In contrast, Chi-Chi (1999, Taiwan), Kocaeli (1999, Türkiye), and Trinidad (2007, USA) represent far-field ground motions, which generally exhibit smoother and more prolonged shaking patterns. Some earthquakes, including Imperial Valley (1979, USA), Northridge (1994, USA), and Friuli (1976, Italy), have relatively short shaking durations, while others such as Landers (1992, USA), Kocaeli, and El Centro show longer and more sustained motions. A few records also display asymmetry in acceleration, with Chi-Chi and Kocaeli showing higher amplitudes in the negative direction, whereas Hollister shows stronger motion in the positive direction. The Fourier amplitude spectra further emphasize these differences. Most records concentrate their seismic energy below 10 Hz, except for the Landers event, which shows pronounced energy between 10 and 15 Hz. Broader spectral content is observed in the Landers, Imperial Valley, and Chi-Chi motions, while Kocaeli, Hollister, and Northridge are dominated by low-frequency components. Records with broader frequency ranges are capable of exciting multiple structural vibration modes,

whereas those dominated by low frequencies mainly affect flexible or long-period structures.

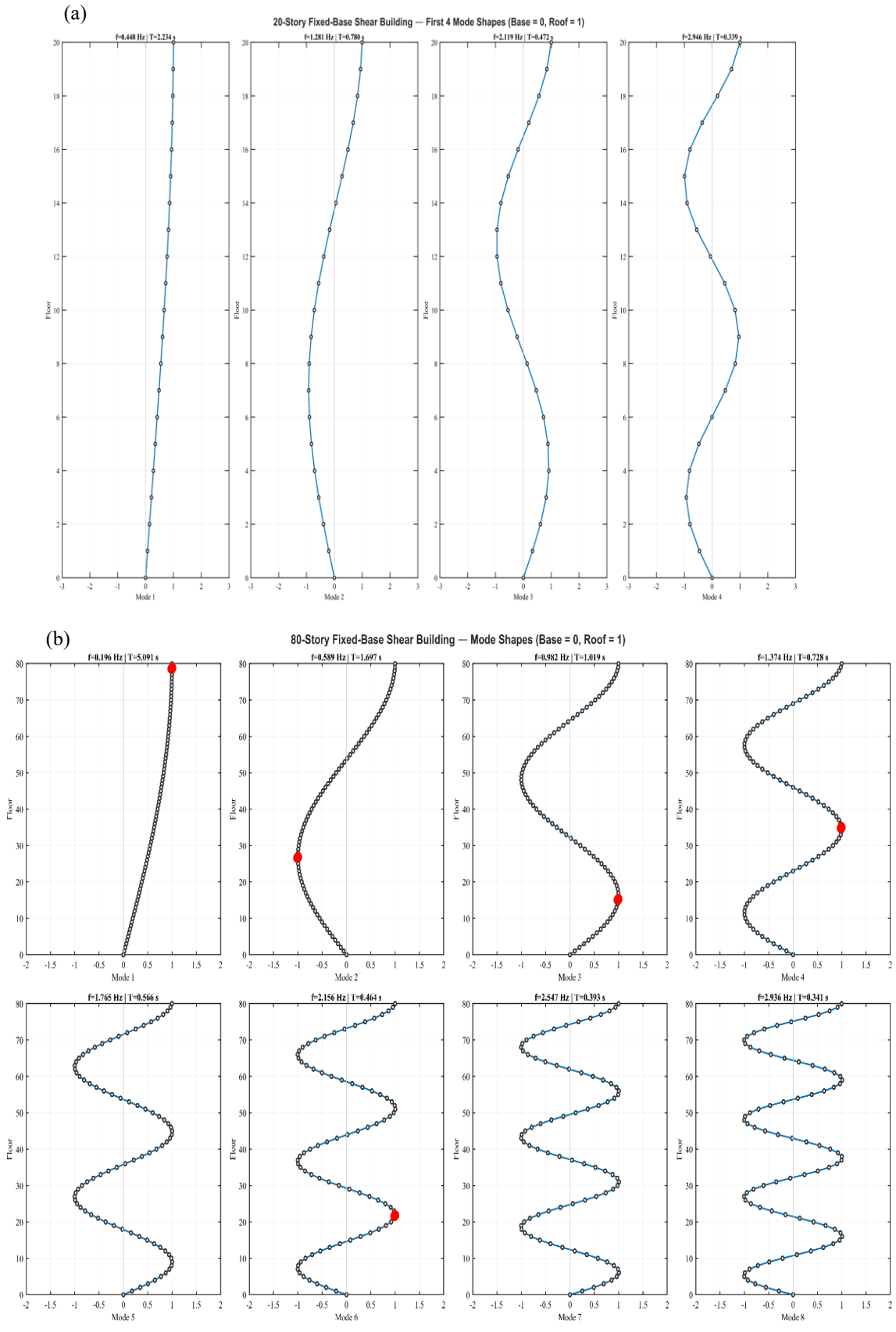

Figure 5. Mode Shape of: (a) 20 Story structure (Case#1); (b) 80 Story structure (Case#2).

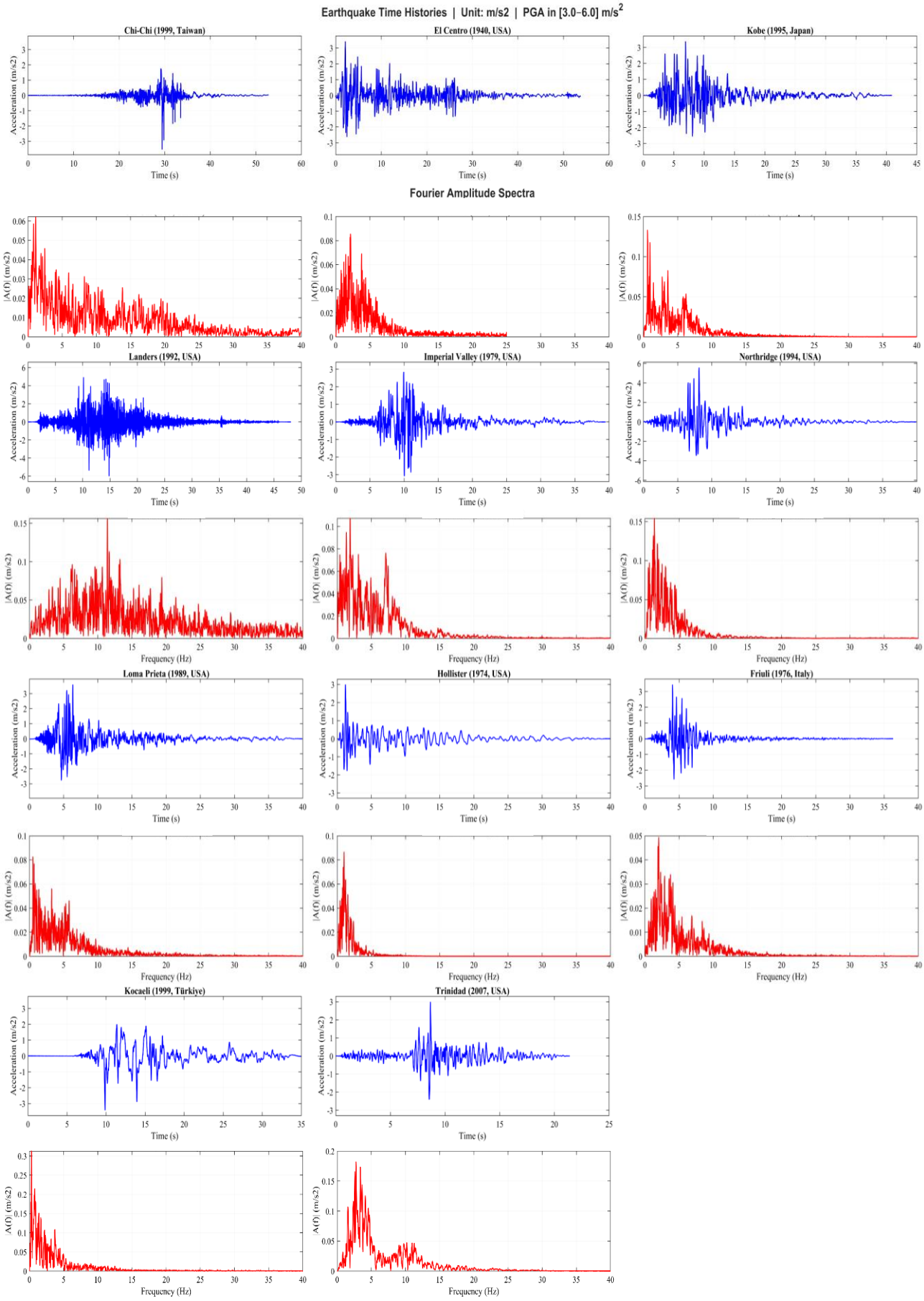

Figure 6. Earthquake with their amplitude spectra considered in this study.

3.2. Case#1 subjected to ground motion controlled by STMD

Figure 7 (a) shows the response of the twenty-story building (case#1) when it is subjected to the El Centro ground motion. The uncontrolled case, shown in gray color, represents the structure without the STMD, while the controlled case, shown in red color, represents the structure equipped with the STMD. It can be clearly seen that the damper effectively reduces the response of the structure. The SRSS response is reduced by 34.9 percent compared with the uncontrolled case. The maximum displacement of the controlled structure is 1.381 meters, which is much smaller than that of the uncontrolled structure. This confirms that the STMD not only reduces the peak response but also decreases the overall structural response. The bottom green dotted line shown in the Figure 7 (b) represents the response of the STMD itself. This response corresponds to the vibration of the additional degree of freedom, the twenty-first, which follows a pattern similar to that of the applied earthquake record.

Figure 7 (c & d) presents the peak and SRSS displacement reduction achieved. The upper subplot (c) plot shows the percentage reduction in peak relative displacement at each floor level, while the lower subplot (d) shows the SRSS reduction of relative displacement, representing the overall vibration energy attenuation across the height of the structure. The peak response shown in light orange indicates that the STMD reduced the peak response at the middle floors by almost 40 percent, while the reduction at the top and bottom floors was less than 30 percent. The translucent pink color represents the SRSS reduction made by the STMD, which remains nearly uniform across all floors with an average reduction of about 37 percent.

Figure 8 shows the response of all stories of the structure when it was subjected to the El Centro earthquake. It can be observed that the response of all stories has been reduced after installing the damper (blue color). The general trend shows that the upper stories experience higher vibration amplitudes compared with the lower stories. This occurs because the upper stories undergo larger motion during dynamic excitation.

Figure 9 presents the relative displacement responses of the 20-story building equipped with the STMD when subjected to three different earthquake records: (a) Chi-Chi, (b) Friuli, and (c) Imperial Valley.

In each case, the black line represents the uncontrolled structure, while the red line represents the controlled response with the STMD. The figure highlights both the peak displacement reduction and the SRSS reduction achieved by the device. For the Chi-Chi earthquake (Figure 9a), the STMD effectively reduces the overall vibration amplitude, achieving an SRSS reduction of about 44.9 percent. The peak displacement (-0.52 m) of the controlled structure is significantly lower than that of the uncontrolled one, indicating good control efficiency under strong ground motion excitation with long-period components.

Under the Friuli earthquake (Figure 9b), the STMD performance is more pronounced, where the SRSS reduction reaches approximately 55.2 percent. The time-history response shows a considerable suppression of oscillations after the initial peak of -0.3335 m, suggesting that the STMD is well tuned to counteract the predominant frequency content of this record. In the case of the Imperial Valley earthquake (Figure 9c), the STMD demonstrates also better control efficiency, with an SRSS reduction of about 50.6 percentage and peak of -1.232 m. The controlled response exhibits a substantial decrease in displacement amplitude throughout the duration, confirming that the STMD effectively mitigates the seismic response.

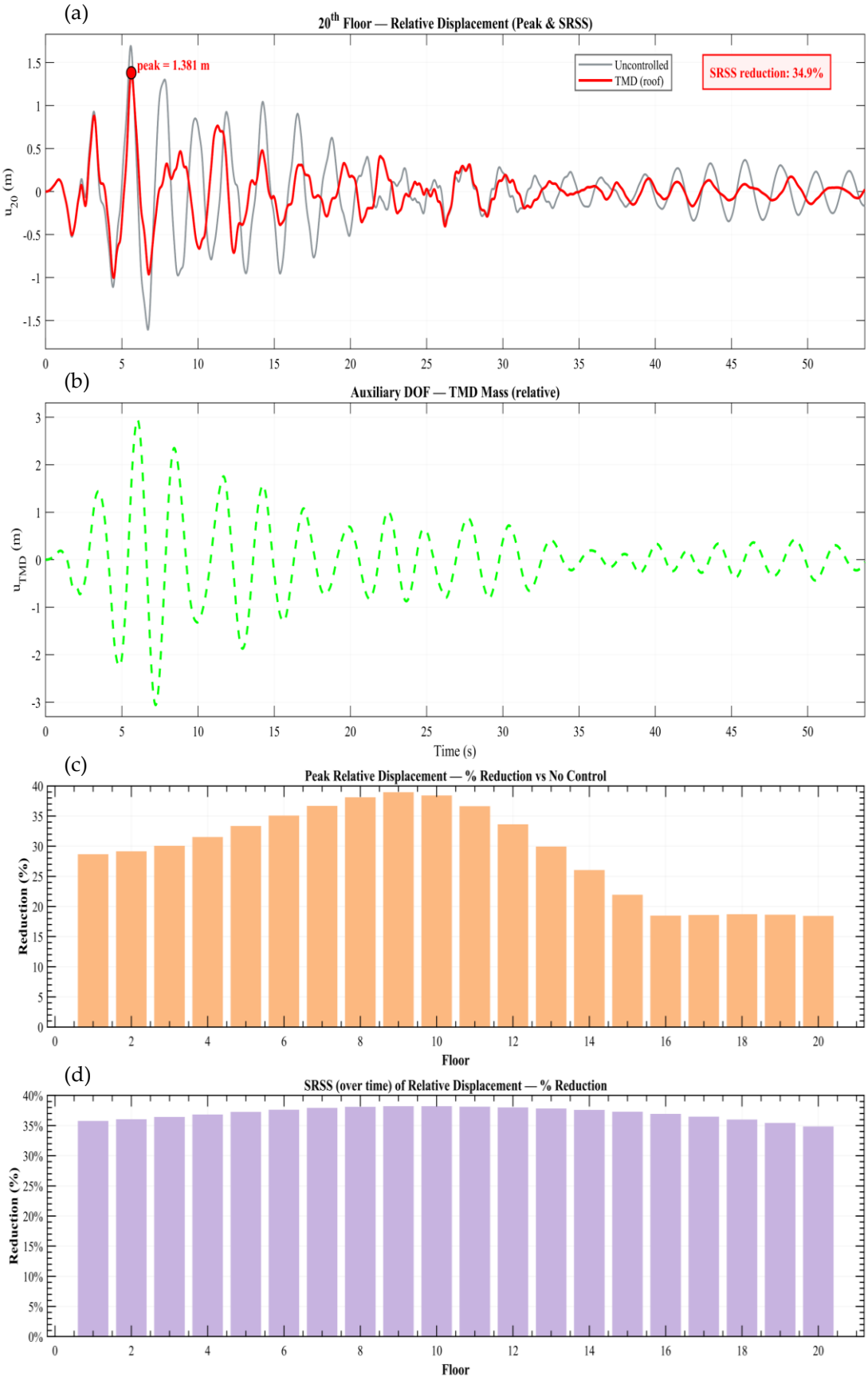

Figure 7. Controlled Case #1: (a) Displacement response of the 20th story, (b) displacement response of the auxiliary system, and reduction achieved by the damper in terms of (c) SRSS and (d) peak response for the structure subjected to the El Centro earthquake.

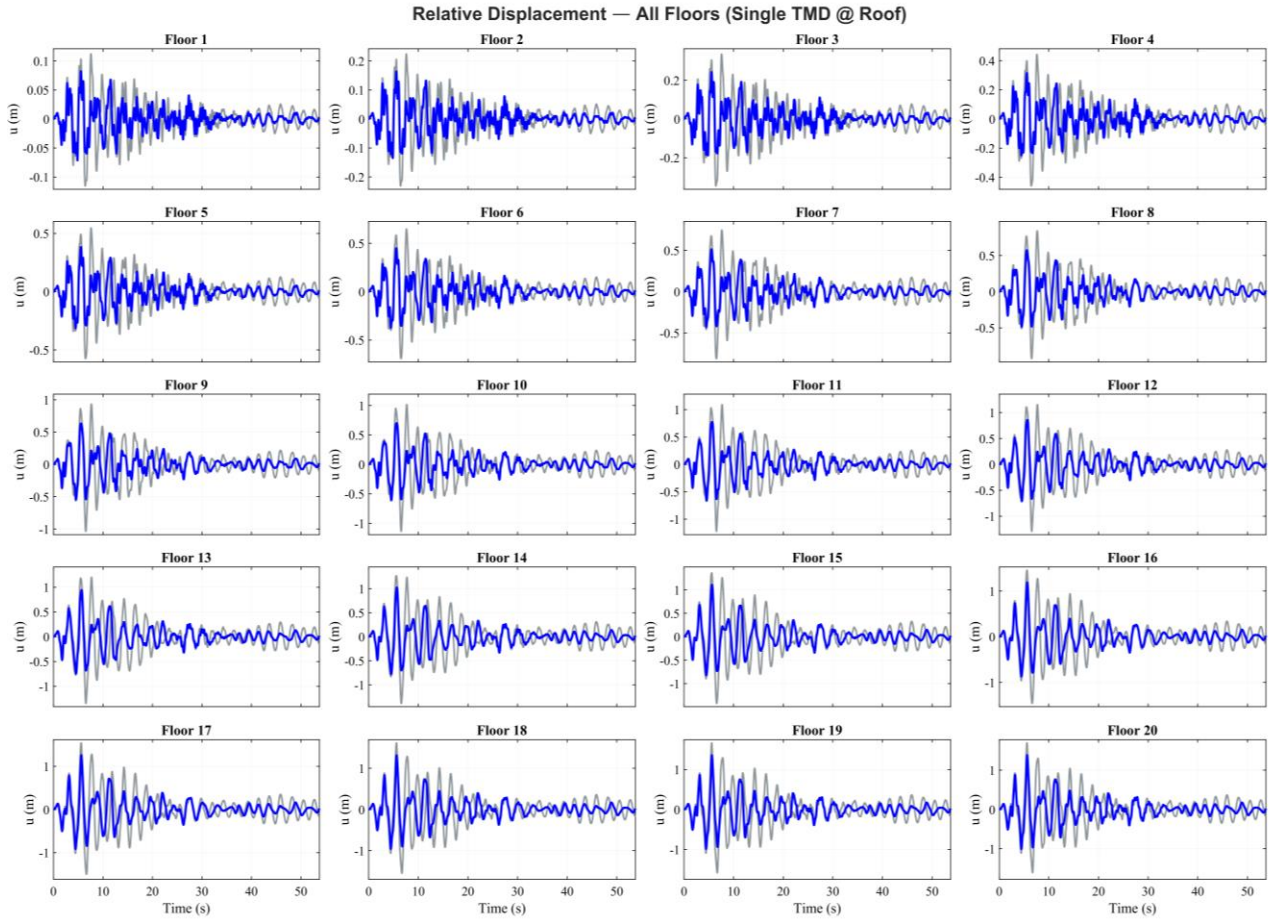

Figure 8. All stories displacement when the structure is subjected to El-Centro.

Figure 10 presents the relative displacement responses of the 20-story building equipped with the STMD when subjected to (a) the Kobe earthquake and (b) the Loma Prieta earthquake. The results clearly illustrate the ability of the STMD to effectively suppress structural vibrations under both strong ground motions.

For the Kobe earthquake (Figure 10a), the peak displacement of the uncontrolled structure reaches approximately -1.082 m, whereas the STMD significantly reduces this value by more than half. The corresponding SRSS reduction is about 52.5 percent, showing that the STMD efficiently mitigates both the instantaneous peak and the overall vibration energy. The damping effect of the STMD is evident, as the oscillations decay more rapidly compared to the uncontrolled case.

Under the Loma Prieta earthquake (Figure 10b), the STMD exhibits even better control performance, achieving an SRSS reduction of nearly 56 percent. The peak displacement is about -1.409 m in the controlled structure.

Figure 11 shows the normalized relative displacement of the STMD installed at the roof of the 20-story building when subjected to different earthquake ground motions, including Chi-Chi, Friuli, Imperial Valley, Kobe, and Loma Prieta. Each curve represents the time-history response of the STMD under a specific earthquake, normalized with respect to its own peak displacement, allowing for direct comparison of the damper behavior across different excitations.

From the figure, it can be observed that the Chi-Chi earthquake produces the largest normalized response amplitude, characterized by long-duration and low-frequency oscillations. This indicates that the Chi-Chi ground motion has a dominant low-frequency content.

The Friuli and Imperial Valley responses exhibit more frequent oscillations with smaller normalized amplitudes, implying that these ground motions contain higher-frequency components. For the Kobe and Loma Prieta earthquakes, the responses remain relatively compact in amplitude and duration, suggesting that the STMD quickly stabilizes after the initial strong motion. The damper maintains effective control without large relative displacements.

The figure 12 presents the comparative response of the structure equipped with a TMD located at the roof level a nd the corresponding uncontrolled case. Each subfigure represents the normalized peak relative displacement along the building height when subjected to distinct ground motions: (a) Chi-Chi, (b) Friuli, (c) Imperial Valley, (d) Kobe, and (e) Loma Prieta earthquakes.

In all cases, the red curves denote the controlled responses, while the black curves correspond to the uncontrolled responses. The controlled configurations consistently demonstrate significant suppression of interstory displacement across the upper floors, confirming the TMD's effectiveness in mitigating vibration amplitudes. The improvement is most pronounced in the top stories, where the influence of the absorber is dominant. The slight variations in reduction patterns among different excitations indicate the dependence of control performance on the spectral characteristics of each earthquake record

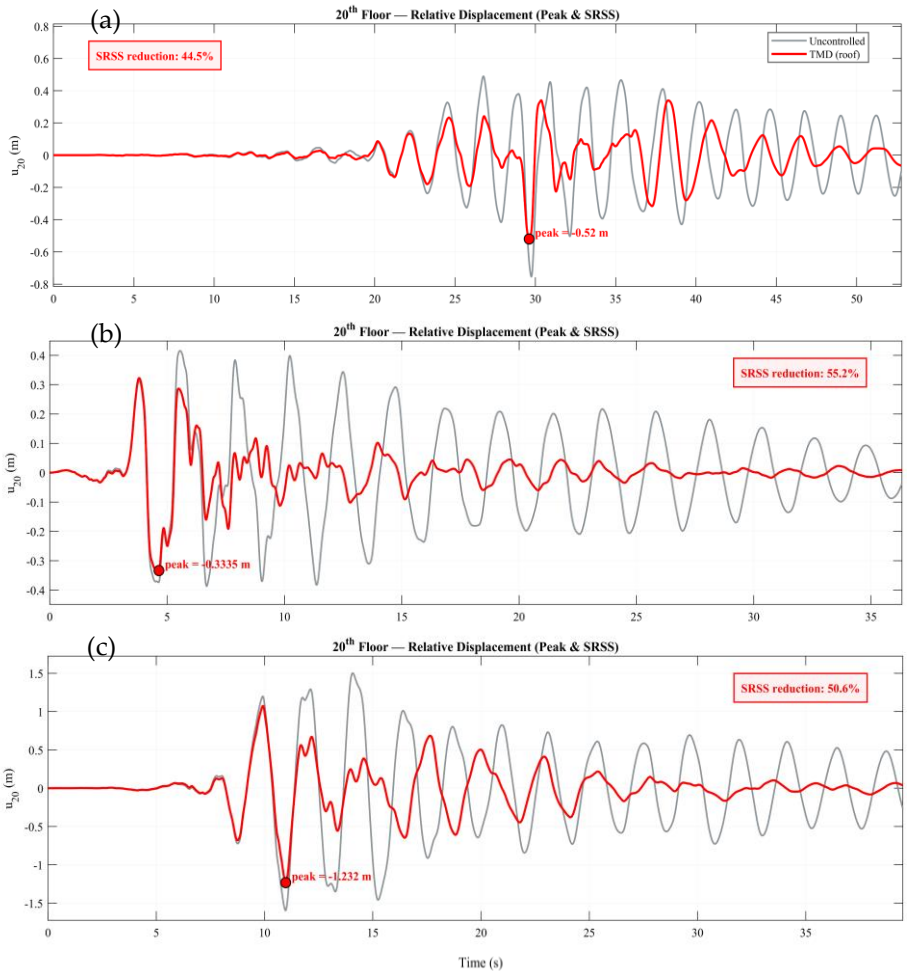

Figure 9. 20 story building equipped with STMD subject to: (a) ChiChi; (b) Friuli and (c) Imperial Valley.

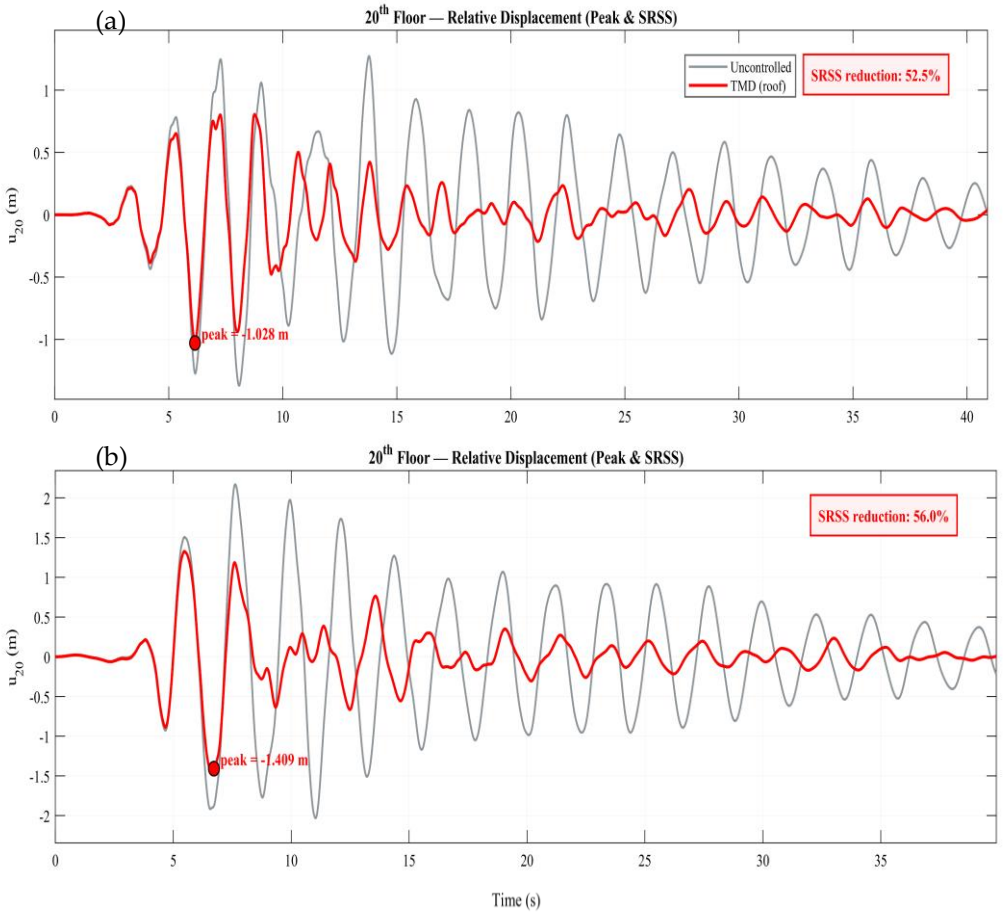

Figure 10. 20 story building equipped with STMD subject to: (a) Kobe and (b) Loma Prieta.

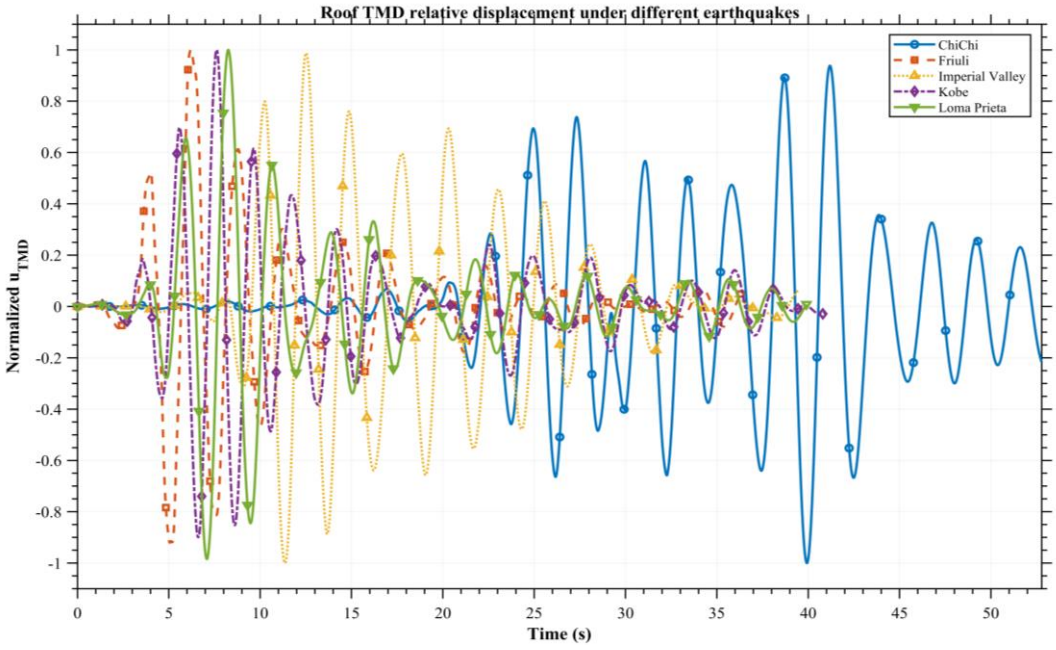

Figure 11. 20 story building STMD normalized by peak displacement when subject to different ground motions.

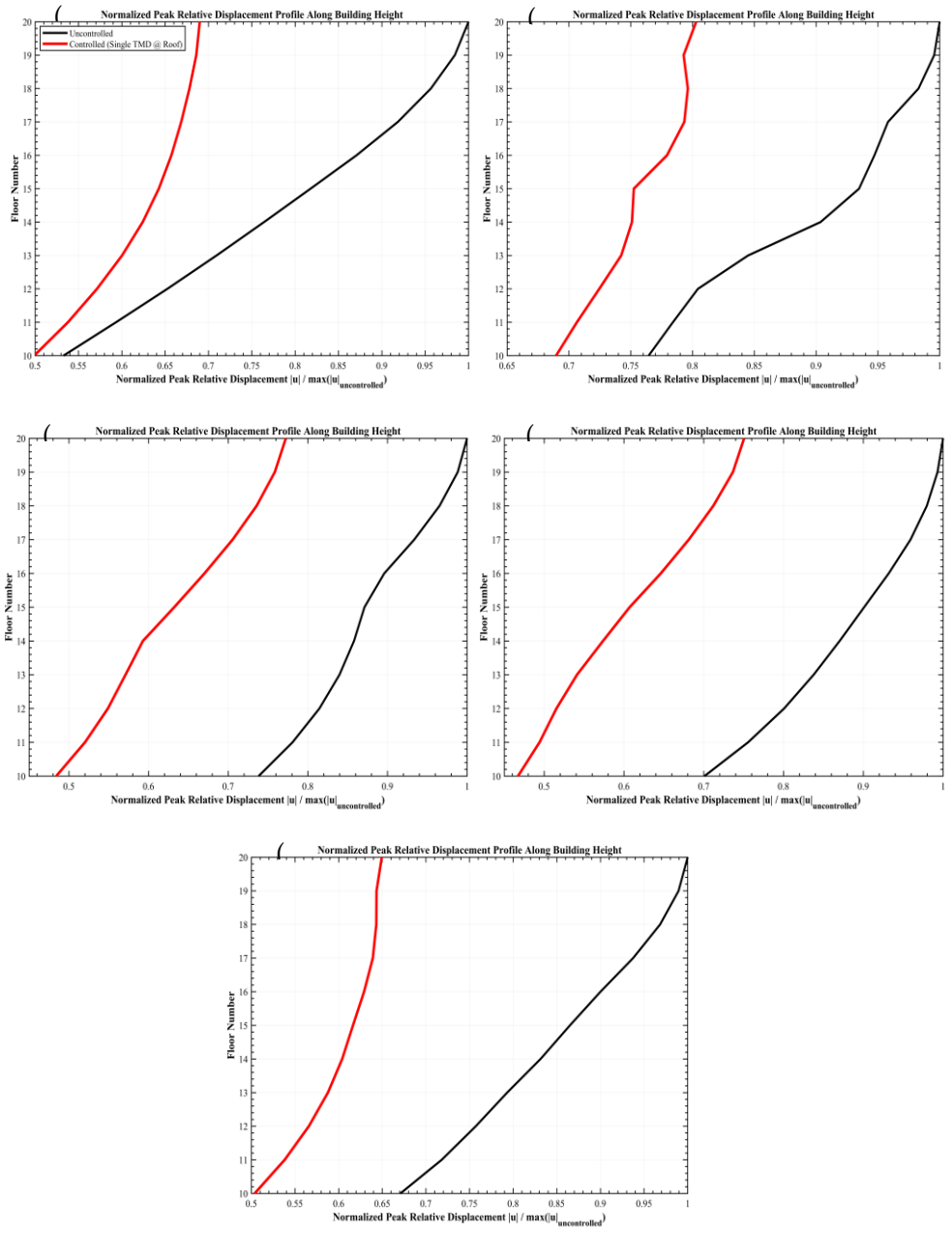

Figure 12. Normalized response of top 10 stories of case#1in uncontrolled and controlled configuration when subjected to: (a) ChiChi; (b) Friuli; (c) Imperial Valley; (d) Kobe and (e) Loma Prieta.

Figure 13 illustrates the percentage reduction in peak and SRSS relative displacements achieved by the STMD when the 20-story shear building was subjected to the different considered earthquakes. Subplot (a) presents the variation in peak relative displacement reduction along the building height, while subplot (b) shows the SRSS (over time) reduction of relative displacement for the same cases.

In subplot (a), the orange (Friuli) bars indicate a non-uniform control pattern, with the lower-middle stories showing smaller reductions (~8–10 %) compared to the lower floors (12–15 %). The blue (Imperial Valley) bars show a steadily decreasing reduction trend from the base toward the top. The green (Kobe) bars reach their highest reduction around the mid-height. The purple (Loma Prieta) bars exhibit a more balanced response, with larger reductions at both the lower and upper floors.

Subplot (b) shows that the SRSS reduction remains nearly constant across all four earthquakes at the top stories, maintaining values around 50–55 %. This uniformity indicates that the STMD effectively dissipates the total vibration energy transmitted through the structure regardless of earthquake characteristics, thereby ensuring consistent damping performance and stable control efficiency across the critical height of the building.

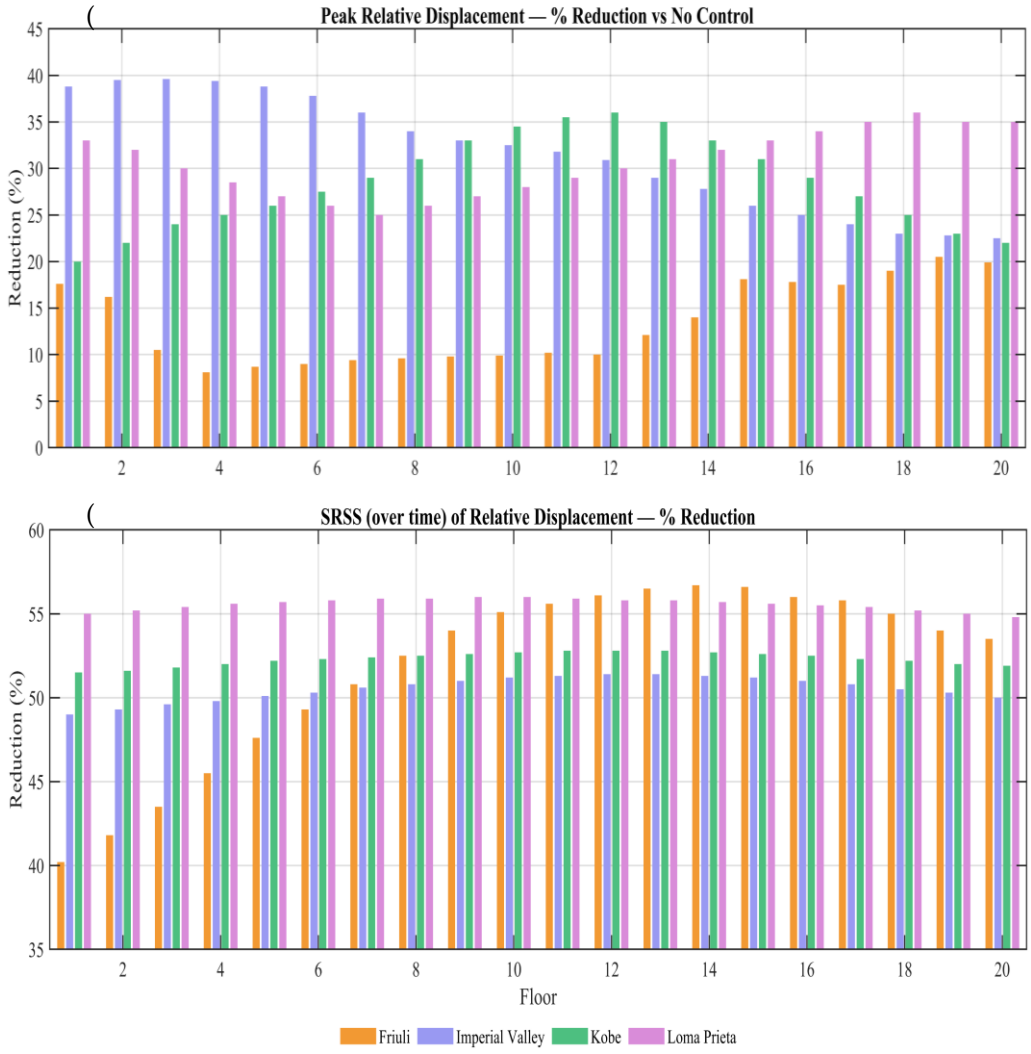

Figure 13. Displacement reduction; (a) Peak and (b) SRSS reduction achieved by the STMD when the case#1 was subjected to different ground excitation.

3.3. Case#2 subjected to wind histories controlled by MTMDs

Figures 14 to 17 present the acceleration responses of an 80-story benchmark building subjected to artificial wind loading. Due to the significant influence of higher vibration modes on the dynamic behavior of such a tall structure, several MTMD configurations were investigated in addition to the STMD case.

In Figure 14, the first subplot, shown in blue, illustrates the response of the structure equipped with a STMD, while the uncontrolled response is plotted in gray. The STMD, tuned to the first mode with a total mass ratio of 5%, achieved an RMS acceleration reduction of 34.9%, with a peak acceleration of approximately 1.007 m/sec^2. Unlike the displacement histories discussed in previous cases, this figure focuses on acceleration histories, as human perception of vibration is primarily governed by acceleration rather than displacement.

The second subplot, represented by the orange curve, corresponds to the configuration with three MTMDs installed at the roof, all tuned to the first mode and sharing a combined mass ratio of 5%. This arrangement resulted in an RMS reduction of 30.1% and a peak acceleration of 1.125 m/sec^2.

The third subplot, shown in yellow, represents the d-MTMD configuration. In this setup, five dampers were installed at floors 80, 35, 27, 22, and 16, corresponding to locations with relatively large modal amplitudes. Each damper was tuned to a specific vibration mode: the first four dampers were tuned to the first four modes, and the fifth was tuned to the sixth mode, as the fifth mode was already effectively controlled by the previously tuned devices. With a total mass ratio slightly above 5%, the d-MTMD system achieved the highest control efficiency, providing an RMS reduction of 35.2% and a peak acceleration of 0.978 m/sec^2.

The fourth subplot, in pink, depicts the arbitrary a-MTMD configuration. Three dampers were installed at floors 60, 40, and 20, with mass ratios of 0.5%, 1%, and 3.5%, respectively, without specific tuning to higher modes. This irregular arrangement yielded a comparatively lower RMS reduction of 21.5% and a peak acceleration of 1.232 m/sec^2.

Figure 15 presents the top-floor acceleration time histories of the same building subjected to a different wind loading pattern (case two) under various control configurations. STMD with a total mass ratio of 5%, effectively reduced the response amplitude, achieving an RMS reduction of 47% and limiting the peak acceleration to 1.172 m/sec^2.

The second subplot which represents three MTMDs achieved almost the same RMS reduction of 47.3%, with a slightly higher peak acceleration of 1.232 m/sec^2, reflecting minor modal interaction among dampers tuned to the same frequency.

The third subplot which is of the d-MTMD configuration effectively suppressed both fundamental and higher-mode responses, achieving an RMS reduction of 47.3% and a peak acceleration of -1.123 m/sec^2.

The bottom subplot shows the a-MTMD configuration, achieved the lowest control efficiency, producing only 24.7% RMS reduction and a peak acceleration of -1.833 m/sec^2

Figure 16 illustrates the building response under a third type of wind loading. The overall trend remains consistent, with the d-MTMD configuration showing superior performance, achieving an RMS reduction of 42.9% and a peak acceleration of -1.057 m/sec^2. The STMD, performing slightly below the d-MTMD, achieved comparable RMS reduction but with a peak acceleration of 1.119 m/sec^2. The MTMDs installed at the roof provided an RMS reduction of 38.9%, with a slightly higher peak acceleration of 1.235 m/sec^2. The a-MTMD configuration again performed the worst, achieving only 28.6% RMS reduction and a peak acceleration of 1.355 m/sec^2.

Figure 17 shows response under a fourth wind loading scenario. The trend here also remains similar, but the overall RMS reductions are lower compared to previous cases, with d-MTMD, STMD, MTMDs at the roof, and a-MTMD achieving reductions of 36.4%, 27.4%, 24.6%, and 17.9%, respectively. Differences in peak acceleration are less pronounced among the first three cases, but the a-MTMD configuration exhibited a notably high peak acceleration of 2.279 m/sec^2. The overall reduced effectiveness of the devices in this case is attributed to the stochastic and irregular nature of the wind load, which likely excited higher vibration modes, leading to these observed conditions. The Table 1 presents the placement rules and mass ratios for different configurations of vibration-controlled devices. It indicates the specific floors at which each type of damper is installed and the corresponding mass ratio relative to the structure. While, Table 2 summarizes the control performance criteria of the dampers. It lists the vibration modes each configuration primarily controls and provides a ranking of their overall effectiveness.

Table 1. The placement rule of vibration-controlled devices.

Configuration Type	Placement (floor)	Mass ratio (%)
STMD	Roof	5
MTMDs@roof	Roof	5
a-MTMDs	60, 40 & 20	5
d-MTMDs	80, 16 27, 35 & 22	5.5

Table 2. The controlment criteria and assessment of the dampers.

Configuration Type	Mode Controlled	Ranking
STMD	1st	2nd
MTMDs@roof	1st	3rd
a-MTMDs	1st	4th
d-MTMDs	1st – 4th & 6th	1st

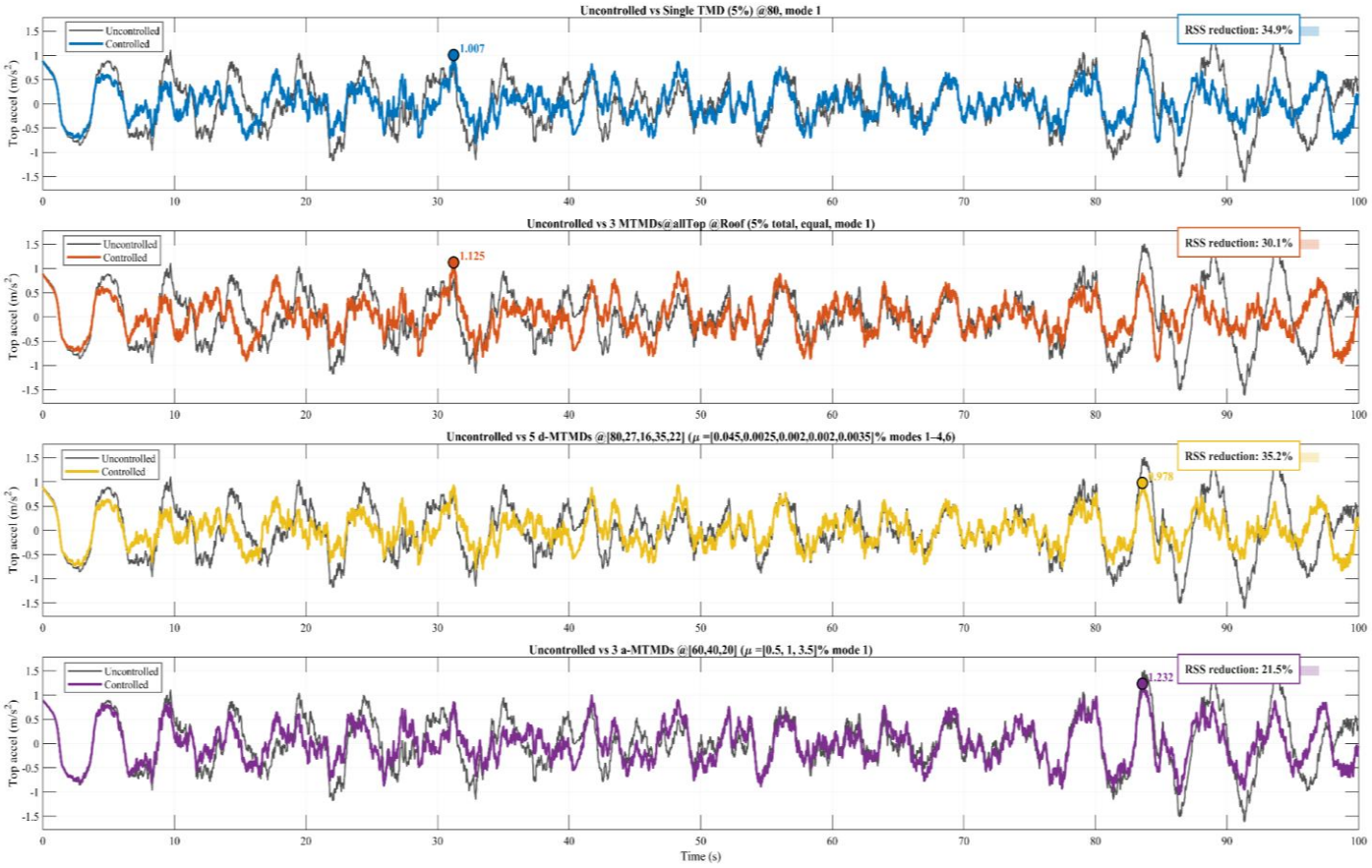

Figure 14. 80 story building uncontrolled and controlled configuration when subject to artificial wind loading case#1.

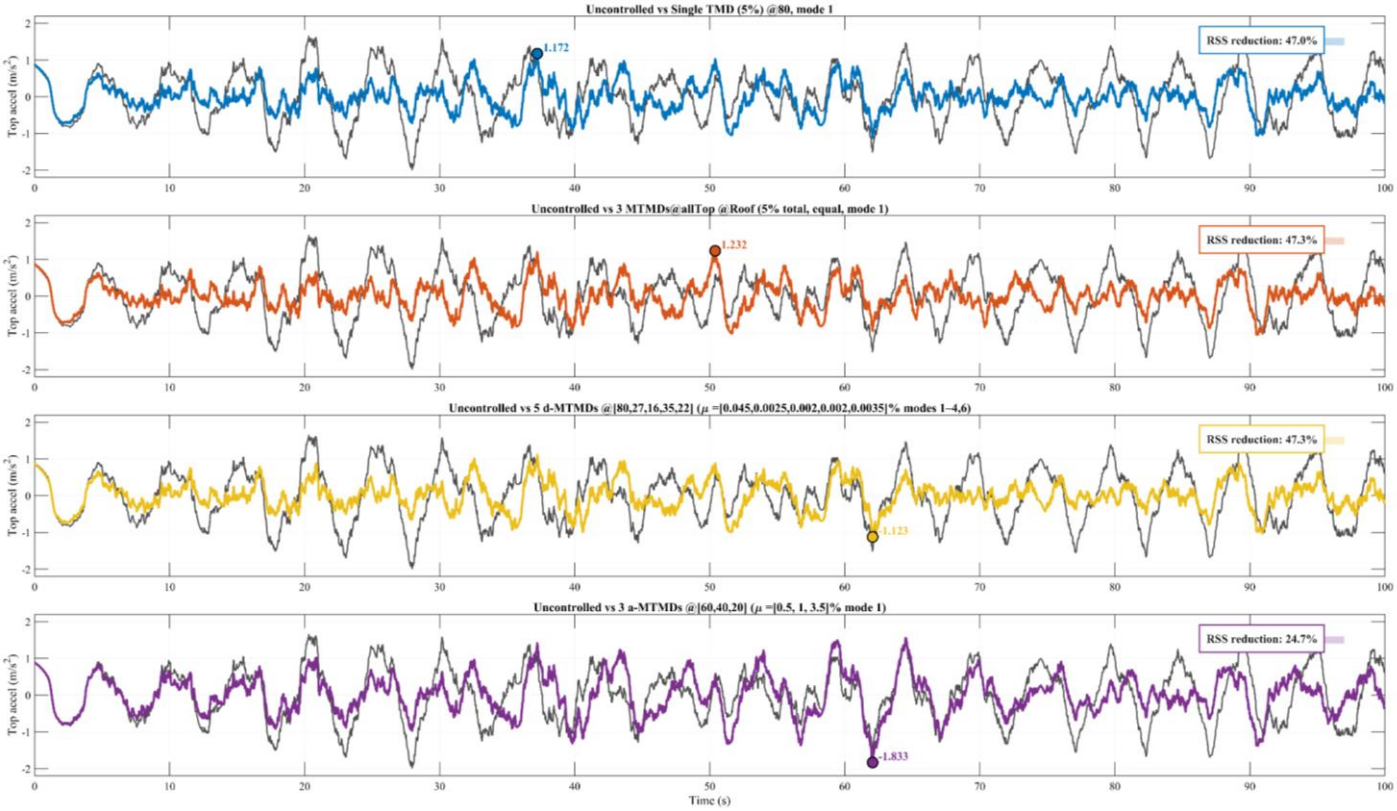

Figure 15. 80 story building uncontrolled and controlled configuration when subject to artificial wind loading case#2.

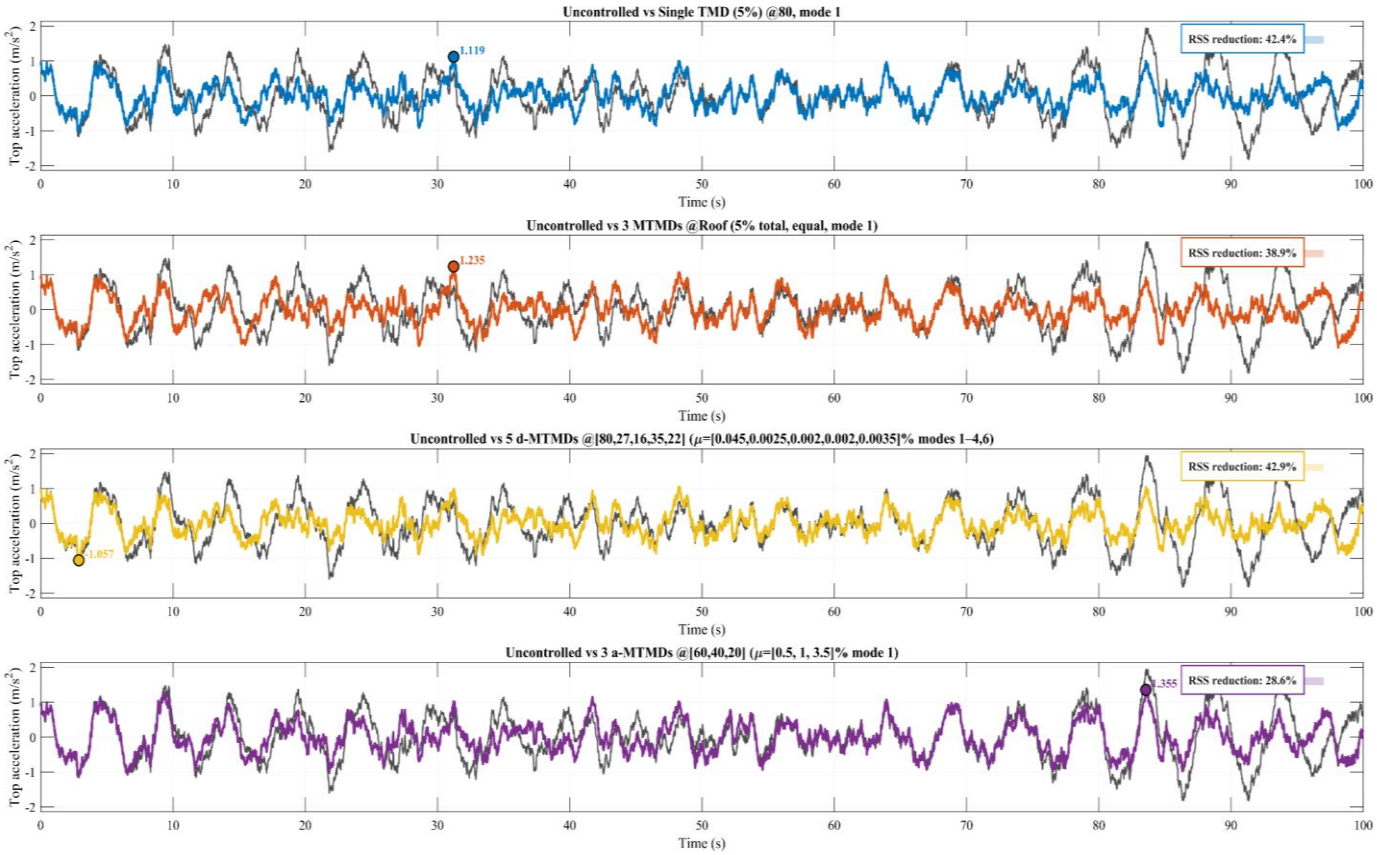

Figure 16. 80 story building uncontrolled and controlled configuration when subject to artificial wind loading case#3

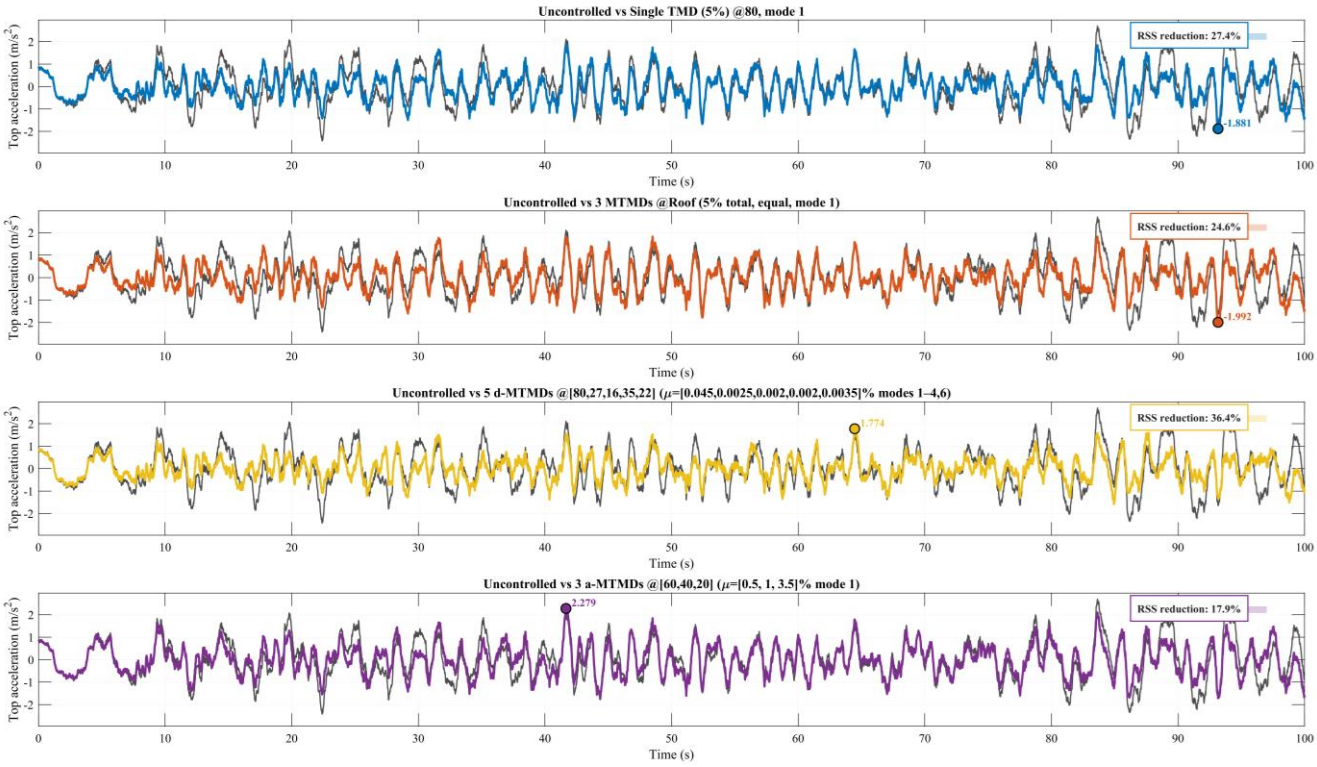

Figure 17. 80 story building uncontrolled and controlled configuration when subject to artificial wind loading case#4

Figure 18 (a) presents the distribution of maximum acceleration for both uncontrolled and controlled configurations of the 80-story structure subjected to Wind Loading Case #1. The controlled STMD and MTMDs arrangement. Each configuration is represented by a distinct line. A curve shifted toward the left indicates a lower acceleration response and, therefore, better performance. The upper stories, particularly above the 10th floor, are of primary importance since they experience the highest accelerations; hence, damping control in this region is critical. The lower ten stories are comparatively less significant as no control device is installed below this level. The 5 d-MTMD configuration demonstrates the most effective performance up to approximately the 60th story, followed by the STMD. Although a slight reduction in control efficiency is observed around upper-mid, the d-MTMD recovers near the top important stories, again surpassing other configurations. The STMD shows consistent performance and becomes the second most effective system, while the 3 MTMDs @ roof rank third. The 3 a-MTMDs provide the least effective control, performing relatively well only around the floors where the absorbers are located due to localized tuning effects. The uncontrolled case exhibits the highest peak accelerations throughout the height, as expected.

Figure 18 (b) shows the corresponding response under Wind Loading Case #3. The overall trend remains consistent, with the d-MTMD system exhibiting the most robust reduction in acceleration, followed sequentially by the STMD, the MTMDs @ roof, and finally the a-MTMDs. In this scenario, the a-MTMDs perform slightly better in the lower stories than the MTMDs @ roof, but their effectiveness diminishes with height.

Figure 18(c) illustrates the results under Wind Loading Case #4, characterized by higher amplitude and rapid frequency fluctuations. The d-MTMDs again outperform other configurations across most of the height, except between the 45th and 55th floors where their efficiency temporarily decreases. Beyond this region, they regain superior performance up to the roof. The STMD remains the next best-performing system and briefly surpasses the d-MTMDs within the 45–55-story range. In contrast, the a-MTMDs

exhibit better control in the lower portion of the structure, whereas the MTMDs @ roof dominate in the upper region.

Figure 19 (a) illustrates the story-wise reduction in acceleration response achieved by each vibration-control configuration in the 80-story benchmark structure subjected to artificial wind loading (Case one). To maintain clarity, only representative stories from the mid-height to the upper portion of the structure are presented, as these regions experience the largest dynamic responses and are therefore of the greatest engineering importance.

The STMD configuration exhibits the most stable and consistent performance in the mid-height stories, achieving a maximum response reduction exceeding 40 %. However, its effectiveness gradually decreases toward both the upper and lower stories. This decline is attributed to the STMD's tuning to the fundamental mode only, which limits its ability to mitigate higher-mode effects that dominate the motion of the upper stories.

The d-MTMD system, comprising five dampers placed at strategically selected floors, demonstrates more uniform control across the structure's height. Although its mid-story performance is marginally lower than that of the STMD, it provides superior attenuation at the top stories, where acceleration amplitudes are highest. This confirms that distributing the dampers across multiple elevations and tuning them to different vibration modes significantly enhances global control efficiency. Consequently, the d-MTMD system emerges as the most effective configuration among all tested cases.

The three roof-mounted MTMDs (3 MTMDs @ roof) achieve a response pattern comparable to that of the STMD but with slightly reduced efficiency. Because all devices are concentrated at the roof and tuned to the same mode, their contribution to suppressing higher-mode effects and lower-story motion remains limited.

The a-MTMD configuration shows improved reduction in the lower stories, primarily due to the placement of most devices at these levels. However, the irregular mass ratios, non-optimized modal tuning, and non-uniform spatial distribution cause its performance to deteriorate in the upper stories, leading to the least effective overall performance among the configurations analyzed.

Figure 19 (b) presents the story-wise acceleration response reductions for the same 80-story structure analyzed previously, but under a different wind loading condition than the previous one (Case two in this plot). The comparison of the two cases allows evaluation of each control configuration's robustness against varying excitation characteristics.

The overall trend observed in the previous Figure remains consistent. The STMD, five d-MTMDs, and 3 MTMDs @ roof all exhibit improved control effectiveness compared with the previous case. In particular, both the STMD and d-MTMDs maintain significant reductions across the mid to upper stories, confirming their stability and adaptability to changes in excitation frequency content.

However, the a-MTMD configuration demonstrates severely degraded performance in this case. Due to the uneven placement, its effectiveness decreases even further compared with that observed previously. The system fails to provide meaningful control.

Since the nature of Wind Loading Type 3 is already been discussed in the Figure 18 (b), its results are not presented here. Instead, the discussion focuses on the other wind loading scenario (case#4), corresponding to the case illustrated in Figure 19 (c). The overall response trend remains consistent with prior observations. The d-MTMD configuration continues to provide the most effective vibration control. Although a slight deterioration in performance is observed at certain time intervals, the system ultimately recovers and maintains a stable control effect. In contrast, the a-MTMD configuration consistently exhibits the weakest performance among all cases.

Because the irregular wind excitation induces stronger participation of higher vibration modes, the superiority of the d-MTMD configuration becomes more pronounced, particularly near the upper region of the structure where higher-mode responses

dominate. This figure therefore reinforces a central conclusion of the study. The performance of MTMD systems is highly sensitive to the optimization strategy adopted for their key design parameters, including the placement of individual dampers, their tuning frequency, and the distribution of their auxiliary masses. When these parameters are selected using a systematic and physically informed optimization procedure, MTMD systems can surpass the conventional STMD approach and deliver significantly enhanced multi-mode vibration mitigation. Conversely, insufficiently optimized MTMD configurations may fail to engage the relevant modes and can result in limited or ineffective control performance.

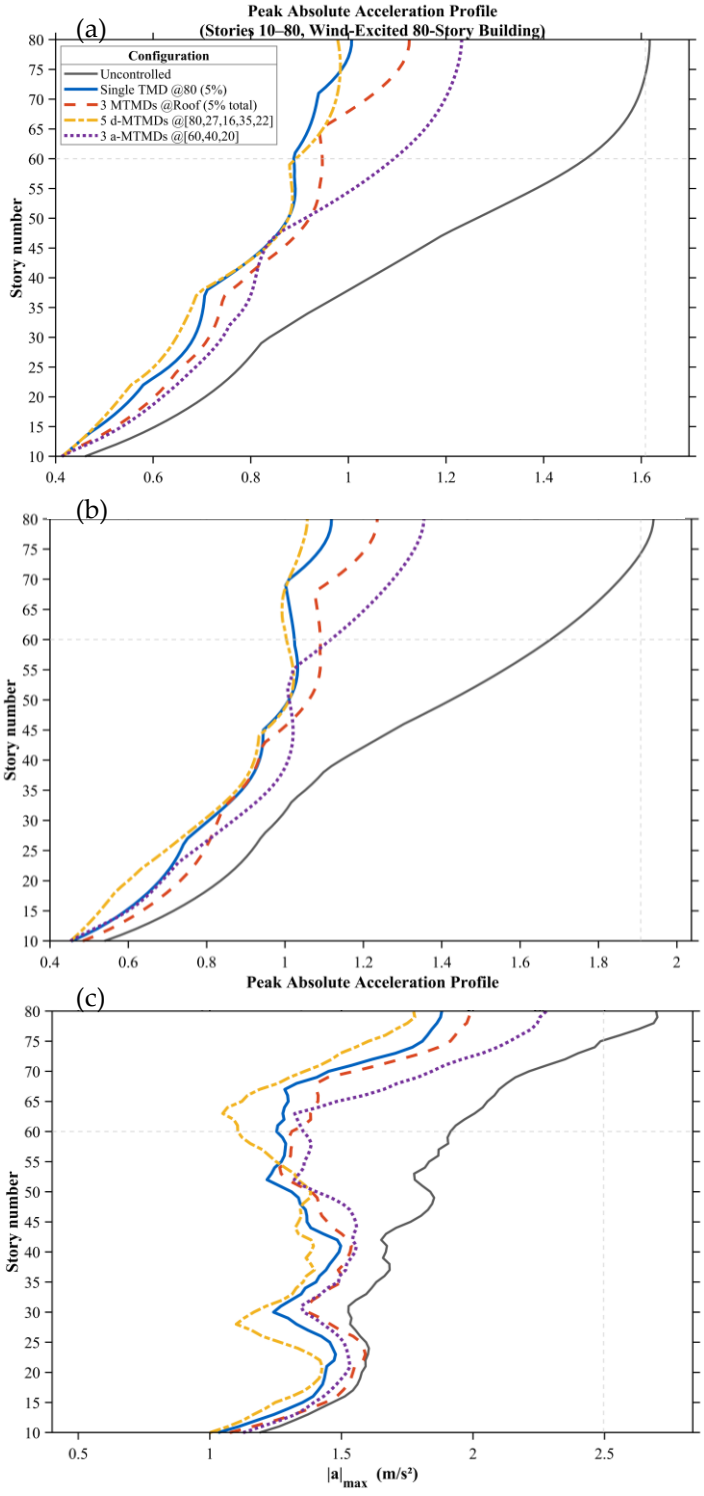

Figure 18. Maximum acceleration per story: (a) case#1; (b) case#3 and (c) case#4.

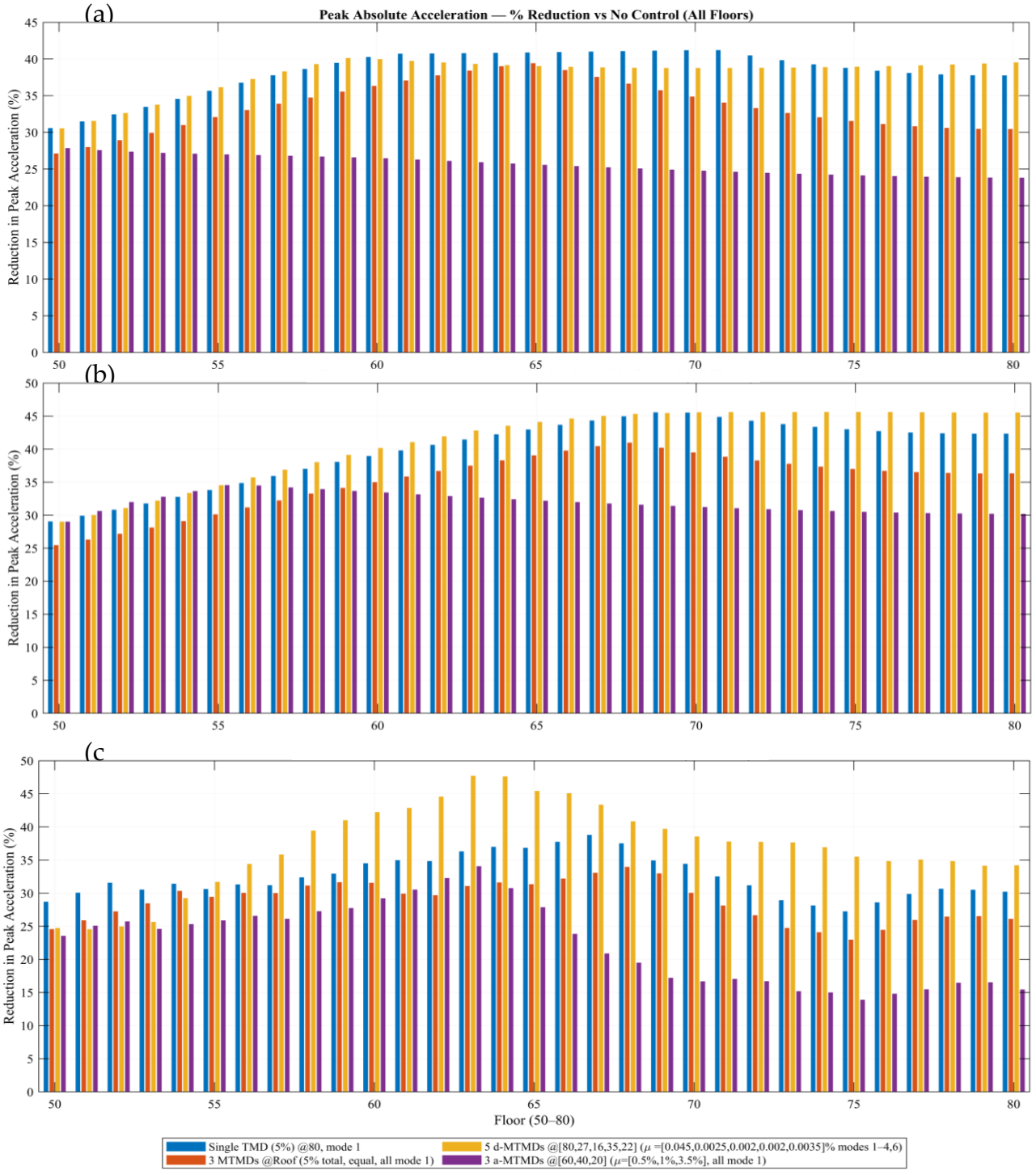

Figure 19. Per floor reduction made by the STMD and MTMDs when the structure was subjected to the artificial wind loading (a) case#1 and (b) case#2; (c) case#4.

4. Conclusion

The present study comprehensively investigated the performance of single and multiple TMDs systems for vibration control in MDOF structures subjected to wind and earthquake excitations. Two representative structural models were analyzed: a 20-story medium-rise building controlled by a STMD under seismic loading and an 80-story high-rise benchmark structure equipped with MTMDs configurations under artificial wind loading. The study aimed to assess how different TMD arrangements influence structural

response reduction and to identify the most efficient configuration for multimodal vibration suppression.

The results from the 20-story model confirmed that the STMD, when properly tuned to the fundamental frequency, effectively mitigates vibrations dominated by the first mode. Significant reductions were observed in both peak and SRSS displacements across all stories, demonstrating the suitability of the STMD for low- and medium-rise buildings where higher-mode effects are negligible. The STMD achieved an average SRSS reduction exceeding 50%, confirming its capability to provide stable and reliable control during various earthquake excitations.

In contrast, for the 80-story high-rise building, higher-mode contributions were found to play a dominant role in the overall dynamic response. Consequently, MTMDs systems were introduced and examined through three configurations: (i) MTMDs@roof, (ii) d-MTMDs, and (iii) a-MTMDs placed without specific tuning rules. Comparative analyses under several wind loading cases revealed that the distributed configuration consistently provided the most balanced and robust control performance. The d-MTMDs achieved the highest reductions in both peak and RMS accelerations, demonstrating superior multimodal energy dissipation due to optimized placement and tuning across dominant vibration modes. The MTMDs@roof configuration provided reasonable but less uniform control, whereas the a-MTMDs exhibited irregular and less reliable performance because of their non-optimized tuning and spatial distribution.

Overall, the findings highlight that the effectiveness of vibration control systems strongly depends on both spatial placement and modal tuning of the dampers. While a STMD is sufficient for short and moderately tall structures governed by a single dominant mode, tall and flexible structures require multiple dampers distributed across several elevations and tuned to different natural frequencies to ensure comprehensive control. The d-MTMDs approach not only enhances energy transfer among vibration modes but also improves the overall structural comfort and serviceability under stochastic excitations such as wind.

Future research should focus on optimizing MTMDs parameters through advanced algorithms, exploring hybrid active–passive configurations, and evaluating real-time adaptability of damper properties under changing excitation characteristics. Incorporating uncertainties in loading and material properties into the optimization framework would further strengthen the reliability and applicability of MTMDs systems for next-generation high-rise and long-span structures.

Data Availability Statement: Available on request.

Acknowledgments: The authors would like to thank the Chinese Scholarship Council (CSC) for providing the scholarship to study at Tongji University, Shanghai, China.

Conflicts of Interest: The authors declare that they have no conflict of interest.

Abbreviations

The following abbreviations are used in this manuscript:

DVAs	Dynamic vibration absorbers
TMDs	Tuned mass dampers
STMD	Single TMD
MTMD	Multi-TMD
d-MTMDs	Distributed MTMDs
a-MTMDs	Arbitrary MTMDs
MTMDs@top	MTMDs all at the roof
SRSS	Square-root-sum-of-squares

RMS	Root-mean-square
TLD	Tuned Liquid Damper
RTHT	Real-Time Hybrid Testing
SDOF	Single-degree-of-freedom
DSFD	Double-Skin Façade Damping
RMS	root-mean-square
MDOF	Multi-degree-of-freedom
RSS	Root-Sum-Square

References

[1] H. Frahm, "Device for damping vibration of bodies," U.S. Patent 989,958, 1909. [Online]. Available: https://patents.google.com/patent/US989958A/en

[2] J. P. Den Hartog, Mechanical Vibrations, 4th ed. New York, NY, USA: McGraw-Hill, 1956.

[3] A. H. Chowdhury and M. D. Iwuchukwu, "The past and future effectiveness of tuned mass dampers," in Proc. 2nd Int. Symp. Struct. Control, The Hague, The Netherlands, vol. 1, pp. 105–127, 1987.

[4] J. Wang, C. Zhang, and Y. Zheng, "An inerter-enhanced asymmetric nonlinear energy sink for response mitigation of structures subjected to harmonic and seismic ground excitations," Struct. Control Health Monit., vol. 29, no. 12, p. e3104, 2022, doi: 10.1002/stc.3104.

[5] T. Horiuchi, M. Inoue, T. Konno, and Y. Namita, "Real-time hybrid experimental system with actuator delay compensation and its application to a piping system with energy absorber," Earthq. Eng. Struct. Dyn., vol. 28, no. 10, pp. 1121–1141, 1999.

[6] A. Najeeb, A. Yasin, and S. Hashim, Seismic vibration control through passive system, B.Sc. thesis, Int. Islamic Univ. (IIUI), Islamabad, 2022. [Online]. Available: https://doi.org/10.13140/RG.2.2.10304.24327

[7] A. Najeeb and M. Y. Jalal, "Dynamic response modeling of SDOF systems using neural networks: A comparative study of ANN and LSTM," in 7th Conf. Sustain. Civil Eng. (CSCE'25), Islamabad, Pakistan, 2025. [Online]. Available: https://www.researchgate.net/publication/395710594

[8] E. O. Ayorinde and G. B. Warburton, "Minimizing structural vibrations with absorbers," Earthq. Eng. Struct. Dyn., vol. 8, no. 3, pp. 219–236, 1980.

[9] K. Iwanami and K. Seto, "Optimum design of dual tuned mass dampers and their effectiveness," Proc. JSME (C), vol. 50, no. 449, pp. 44–52, 1985 (in Japanese).

[10]A. Kareem and S. Kline, "Performance of multiple tuned mass dampers under random loading," J. Struct. Eng., vol. 121, no. 2, pp. 348–361, 1995.

[11]Y. M. Ram and S. Elhay, "Theory of a MTMD dynamic absorber," J. Vib. Control, vol. 2, no. 5, pp. 607–616, 1996.

[12]A. S. Joshi and R. S. Jangid, "Optimum parameters of multiple tuned mass dampers for base-excited damped systems," J. Sound Vib., vol. 202, no. 5, pp. 657–667, 1997.

[13]R. S. Jangid, "Dynamic characteristics of structures with multiple tuned mass dampers," Struct. Eng. Mech., vol. 3, no. 5, pp. 497–509, 1995.

[14]R. S. Jangid, "Optimum multiple tuned mass dampers for base-excited undamped system," Earthquake Eng. Struct. Dyn., vol. 28, no. 9, pp. 1041–1049, 1999.

[15]V. D. Blondel and J. N. Tsitsiklis, "A survey of computational complexity results in systems and control," Automatica, vol. 36, no. 9, pp. 1249–1274, 2000.

[16]C. Li, "Performance of multiple tuned mass dampers for attenuating undesirable oscillations of structures under ground acceleration," Earthquake Eng. Struct. Dyn., vol. 29, no. 9, pp. 1405–1421, 2000.

[17]C. Li and Y. Liu, "Further characteristics for multiple tuned mass dampers," J. Struct. Eng., vol. 128, no. 10, pp. 1362–1365, 2002.

[18]C. Li and Y. Liu, "Optimum multiple tuned mass dampers for structures under the ground acceleration based on the uniform distribution of system parameters," Earthquake Eng. Struct. Dyn., vol. 32, no. 5, pp. 671–690, 2003.

[19]T. Wen and B. Zou, "Time and frequency domain analysis of substructure characteristics on dynamic structure," J. Archit. Sci. Eng., vol. 23, pp. 78–84, 2003.

[20]C. Li and J. Zhang, "Evaluation of arbitrary integer based multiple tuned mass dampers for structures," Int. J. Struct. Stab. Dyn., vol. 5, no. 3, pp. 475–488, 2005.

[21]C. Li and Q. S. Li, "Evaluation of the lever-type multiple tuned mass dampers for mitigating harmonically forced vibration," Int. J. Struct. Stab. Dyn., vol. 5, no. 4, pp. 641–664, 2005.
[22]B. Han and C. Li, "Evaluation of multiple dual tuned mass dampers for structures under harmonic ground acceleration," Int. J. Struct. Stab. Dyn., vol. 6, no. 1, pp. 59–75, 2006.
[23]C. Li, "Estimation of dual-layer multiple tuned mass dampers for structures under ground acceleration," Int. J. Struct. Stab. Dyn., vol. 6, no. 4, pp. 541–557, 2006.
[24]C. Li and B. Zhu, "Estimating double tuned mass dampers for structures under ground acceleration using a novel optimum criterion," J. Sound Vib., vol. 298, no. 1–2, pp. 280–297, 2006.
[25]H.-N. Li and X.-L. Ni, "Optimization of non-uniformly distributed multiple tuned mass damper," J. Sound Vib., vol. 308, no. 1–2, pp. 80–97, 2007.
[26]B. Han and C. Li, "Evaluation of multiple dual tuned mass dampers for structures under harmonic ground acceleration," Int. J. Struct. Stab. Dyn., vol. 6, no. 1, pp. 59–75, 2006.
[27]B. Han and C. Li, "Characteristics of linearly distributed parameter-based multiple-tuned mass dampers," Struct. Control Health Monit., vol. 15, no. 6, pp. 839–856, 2008.
[28]S.-Y. Ok, J. Song, and K.-S. Park, "Development of optimal design formula for bi-tuned mass dampers using multi-objective optimization," J. Sound Vib., vol. 322, no. 1–2, pp. 60–77, 2009.
[29]Y. M. Parulekar and G. R. Reddy, "Passive response control systems for seismic response reduction: A state-of-the-art review," Int. J. Struct. Stab. Dyn., vol. 9, no. 1, pp. 151–177, 2009.
[30]L. Zuo, "Effective and robust vibration control using series multiple tuned–mass dampers," J. Vib. Acoust., vol. 131, no. 3, pp. 0310031–03100311, 2009.
[31]C. C. Lin, J. F. Wang, C. H. Lien, H. W. Chiang, and C. S. Lin, "Optimum design and experimental study of multiple tuned mass dampers with limited stroke," Earthquake Eng. Struct. Dyn., vol. 39, no. 14, pp. 1631–1651, 2010.
[32]Y. Yang, J. Munoa, and Y. Altintas, "Optimization of multiple tuned mass dampers to suppress machine tool chatter," Int. J. Mach. Tools Manuf., vol. 50, no. 9, pp. 834–842, 2010.
[33]M. Jokic, M. Stegic, and M. Butkovic, "Reduced-order multiple tuned mass damper optimization: A bounded real lemma for descriptor systems approach," J. Sound Vib., vol. 330, no. 2, pp. 5259–5268, 2011.
[34]L. A. Bergman, D. M. McFarland, J. K. Hall, E. A. Johnson, and A. Kareem, "Optimal distribution of tuned mass dampers in wind sensitive structures," in Struct. Safety Reliab.: Proc. ICOSSAR'89, New York, NY, USA, pp. 95–102, 1989.
[35]M. Feng and A. Mita, "Vibration control of tall buildings using mega sub-configuration," J. Eng. Mech., vol. 121, no. 10, pp. 1082–1088, 1995.
[36]F. Sadek, B. Mohraz, A. W. Taylor, and R. M. Chung, "A method of estimating the parameters of tuned mass dampers for seismic application," Earthquake Eng. Struct. Dyn., vol. 26, no. 5, pp. 617–635, 1997.
[37]G. Chen and J. Wu, "Optimal placement of multiple tuned mass dampers for seismic structures," J. Struct. Eng., vol. 127, no. 9, pp. 1054–1062, 2001.
[38]J. Wu and G. Chen, "Optimization of multiple tuned mass dampers for seismic response reduction," in Amer. Control Conf., Chicago, IL, USA, pp. 519–523, 2000.
[39]F. Petit, M. Loccufier, and D. Aeyels, "On the attachment location of dynamic vibration absorbers," J. Vib. Acoust., vol. 131, no. 3, pp. 034501-1–034501-8, 2009.
[40]M. M. Ali and K. Moon, "Structural developments in tall buildings: Current trends and future prospects," Archit. Sci. Rev., vol. 50, no. 3, pp. 205–223, 2007.
[41]K. S. Moon, "Vertically distributed multiple tuned mass dampers in tall buildings: Performance analysis and preliminary design," Struct. Design Tall Spec. Build., vol. 19, no. 3, pp. 347–366, 2010.
[42]T. S. Fu and E. A. Johnson, "Control strategies for a distributed mass damper system," in Amer. Control Conf. (ACC2009), St. Louis, MO, USA, June 10–12, 2009.
[43]T. S. Fu and E. A. Johnson, "Distributed mass damper system for integrating structural and environmental controls in buildings," J. Eng. Mech., vol. 137, no. 3, pp. 205–213, 2011.
[44]P. Xiang and A. Nishitani, "Seismic vibration control of building structures with multiple tuned mass damper floors integrated," Earthquake Eng. Struct. Dyn., vol. 43, no. 6, pp. 909–925, 2014.
[45]S. Elias and V. Matsagar, "Wind response control of a 76-storey benchmark building installed with distributed multiple tuned mass dampers," J. Wind Eng., vol. 11, no. 2, pp. 37–49, 2014.

[46]S. Elias and V. Matsagar, "Distributed multiple tuned mass dampers for wind vibration response control of high-rise building," J. Eng., [Online]. Available: http://www.hindawi.com/journals/je/aip/198719
[47]K. S. Moon, "Integrated damping systems for tall buildings: Tuned mass damper/double skin facade damping interaction system," Struct. Design Tall Spec. Build., vol. 25, no. 5, pp. 232–244, 2015.
[48]S. Elias, V. Matsagar, and T. K. Datta, "Effectiveness of distributed tuned mass dampers for multi-mode control of chimney under earthquakes," Eng. Struct., vol. 124, pp. 1–16, 2016, doi: 10.1016/j.engstruct.2016.06.006.
[49]S. Elias and V. Matsagar, "Wind response control of tall buildings with a tuned mass damper," J. Build. Eng., 2017.
[50]S. Elias, V. Matsagar, and T. K. Datta, "Distributed tuned mass dampers for multi-mode control of benchmark building under seismic excitations," J. Earthquake Eng., vol. 23, no. 7, pp. 1137–1172, 2019, doi: 10.1080/13632469.2017.1351407.s
[51]S. Djerouni, S. Elias, M. Abdeddaim, and R. Rupakhety, "Multi-tuned mass damper inerter (MTMDI) system for earthquake-induced vibration control of buildings," Eng. Struct., vol. 313, p. 119139, 2024, doi: 10.1016/j.engstruct.2024.119139.